nature portfolio

Peer Review File

Promoting OH Cycle on Activated Dynamic Interface for Electrocatalytic Ammonia Synthesis

REVIEWER COMMENTS

Reviewer #1 (Remarks to the Author):

The manuscript reported an OH cycle mechanism regarding the formation of a local-hydroxyl-enrich nanoconfined reaction surface to promote the hydrogenation process of nitrate. Then by further activating the dynamic state via constructing surface vacancies, the NH3 production activity was achieved with a Faradaic efficiency of almost 100% at wide nitrate concentration. Although the author spends a lot of space explaining the hydroxyl-cycle mechanism, there are still many confusing details. In other words, some conclusions can't be supported. Now, some catalyst could achieve high Faradaic efficiency at a wide range of nitrate concentration. Thus, I think the quality of the manuscript can’t match the demand of Nature Communication. Some concerns need to be stressed.

1. What is the existent form of the stated OH species? OH- or •OH? It is strange to capture •OH species at a strong reduction condition at -0.8 V vs. RHE (Figs. 5e and f). •OH species are usually considered strong oxidants to be used in the Fenton reaction or in eliminating organic pollutants (DOI:10.1021/acs.est.1c00230). Besides, It is confusing that the author stressed the confinement of OH species without pointing out the specific component that plays the role of confinement. Nanoconfining is achieved by partial or complete encapsulation or confinement in nanoscope-level space (i.e. nanoscope-limited space), including nanoscope-level channels, two-dimensional interfaces, pores, and cavities (DOI:10.1007/s10311-021-01355-z).
2. As the author stated in the manuscript, there are hydroxyl vacancies after NTP treatment, it is recommended the authors compare the content of surface Ni-OH species through XPS analysis (Nat. Mater. 20, 1240–1247 (2021)).
3. It would be better if the authors provided the raw data of the in situ Raman test in supplementary information. Notably, for Ni(OH)2/Ni@CF, the surface is composed of Ni and Ni(OH)2. For the defect-rich D-Ni(OH) /Ni@CF, the Raman peaks of Ni-OH vanished completely (Fig. 5C). At this time, does the proposed hydroxyl-cycle mechanism work? Then, The name of D-Ni(OH)2/Ni@CF used in the manuscript indicated the formation of a special structure. The author should provide the XRD data to support their idea.
4. In Figure 3b, the authors used FTIR to determine the ratio of deuterium ammonia to ammonia (D/H), but no related FTIR spectra were supplemented either in the main text or in the supplementary information. Besides, considering the complexity of the IR spectrum, online DEMS was more suitable for studying the process of surface OH desorption → limited OH diffusion → OH participation in the hydrogenation(Nat Catal 4, 1012–1023 (2021); DOI:10.1002/smll.202303249).
5. The assignment of Raman peaks in Fig S11 needs to be reconsidered. The peak range from 3200 to 3600 cm-1 is usually related to H2O (Nature Protocols 2023, 18, 883-901; Nature 2021, 600, 81-85). In other words, it is recommended to provide the Raman spectra of standard NH3, ND3, and H2O to support the peak assignment.
6. After NTP treatment, the ECSA of D-Ni(OH)2/Ni@CF increased a lot. The introduction of plasma treatment may introduce holes in the catalysts' surface and enlarge the specific surface area. After normalizing to the ECSA, would D-Ni(OH)2/Ni@CF still own the better activity?
7. The experimental details of the in situ experiment need to be supplemented. For example, if the experimental details of EPR experiments were not controlled, the obtained spectra can not be used to compare the number of defects or the number of generated •OH.

Reviewer #2 (Remarks to the Author):

This manuscript reports an intriguing effect of electrocatalyst-electrolyte interaction on ammonia synthesis. With Ni(OH)2 as the model electrocatalyst, OH cycle was proposed to be involved in the hydrogeneration process of nitrogen species, which is well backed-up by the in-situ characterization and isotope-labeling experiments. The manuscript should be publishable after the following issues been addressed.

1. The authors claimed that the Ni(OH)2 reconstructed into Ni at ~-2.3 V vs. RHE in Figure 3c. However, the working potential was set as 0~-1.0 V vs. RHE in all the subsequent electrochemical experiments. Please comment.

2. The author substantiated the identification of hydroxyl vacancy sites on the catalyst surface through the application of positron annihilation lifetime spectroscopy (PALS) as depicted in Figure 4c. They asserted that the defect relaxation time (τ1) within the range of 114 to 128 ps signifies the emergence of vacancies. Please elaborate or offer more rlated references. What is τ1?

3. The XRD patterns of the electrocatalysts were shown in Figure S3-4 to characterize the phase composition of the catalyst. However, conspicuous peaks corresponding to Cu appeared in the XRD patterns. Can the authors elucidate the cause of this observation? Additionally, whether the Cu forms additional active sites? Does Cu impact on the overall performance of the catalyst.

4. In situ Raman spectroscopy was used to characterize the valence state and phase of the catalyst surface. However, the description of the in-situ Raman method is missing. In addition, the authors did not describe the experimental methods of in situ FTIR and EPR, neither.

5. The authors mentioned COHP calculation in the manuscript, but there was no relevant content in the discussion of the results.

6. HER is perhaps the most important competitive reaction of NO3RR in aqueous environment, and the activity of D-Ni(OH)2/Ni@CF and Ni(OH)2/Ni@CF for HER reaction needs to be demonstrated in detail.

Reviewer #3 (Remarks to the Author):

In this manuscript, a potential-dependent phase change was observed with Ni(OH)2 as the electrocatalyst during nitrate reduction reaction (NO3RR), while an OH cycle mechanism was proposed regarding the formation of a local-hydroxyl-enrich nanoconfined reaction surface to promote hydrogenation process. By further constructing more surface vacancies via plasma treatment, excellent NO3RR performance can be achieved on D-Ni(OH)2/Ni@CF. Despite good NO3RR performance and some new insights from the authors, this reviewer still has several critical comments.

The first is that how the OH from the catalyst participates in/promotes NO3RR to NH3 process, considering that there is much OH in the alkaline electrolyte already? The authors need to give detailed discussion. The second is that is it possible that the as-generated

Ni/Ni(OH)2 with suitable binding energies of reaction intermediates contributes to the good NO3RR performance, rather than OH cycle? This reviewer supposes that when hydroxyl vacancies are introduced in D-Ni(OH)2/Ni@CF, more Ni species are generated during NO3RR, and the as-generated Ni is responsible for water splitting to provide enough H for NO3RR, leading to greatly enhanced NO3RR performance. Overall, the mechanism understanding is not clear at this stage, which needs more exploration and discussion. Some additional suggestions are also listed as below:

1. In this contribution, Cu foam is used as the substrate. Is it possible that Cu atoms dissolve and deposit on or doped in the catalyst for enhanced NO3RR performance, as Cu is generally regarded as a highly active electrocatalyst for NO3RR.
2. The authors claim that structural reconstruction takes place at the top layers of the catalyst surface. However, as shown in fig. 2c, the newly formed Ni is in the inner area, which is coved by surface Ni(OH)2.
3. Please label the XRD peak at near 35 degrees in fig. S4.
4. “This phenomenon demonstrated that the Ni(OH)2/Ni interface was not static, where the metallic Ni readily regenerated into Ni(OH)2 by spontaneously bonding to the hydroxyl group in solvent.” Here, should be Ni(OD)2/Ni, not Ni(OH)2/Ni.
5. As displayed in fig. 3d, Ni(OH)2/Ni surface has a better OH capture ability than Ni. However, the DFT results in fig. S12 only show the free energy diagram of NO3RR process on Ni and Ni(OH)2, while Ni(OH)2/Ni is the real catalyst for NO3RR.
6. The authors demonstrate that the OH or OD from the catalyst participates in NO3RR process. Can the authors explain how OH or OD reacts with NO_3^-, as it is generally suggested that the as-generated NH3 capture the H from the decomposition of H2O.
7. Where is fig. 3e as mentioned by the authors?
8. Is it possible that the enhanced current density of D-Ni(OH)/Ni@CF from the LSV curve is only caused by the larger ECSA (fig. S20)?
9. Pls avoid such simple mistakes like “Upon the addition of 1 M KNO3”, “fig. 5i”, etc.
10. Fig. 6g-h demonstrate the importance of accelerated H2O dissociation kinetic to provide enough H for NO3RR. So does it mean that the H in NH3 mainly comes from the dissociation of water, rather than the OH from the catalyst.

Reviewer #1 (Remarks to the Author):

The manuscript reported an OH cycle mechanism regarding the formation of a local-hydroxyl-enrich nanoconfined reaction surface to promote the hydrogenation process of nitrate. Then by further activating the dynamic state via constructing surface vacancies, the NH_3 production activity was achieved with a Faradaic efficiency of almost 100% at wide nitrate concentration. Although the author spends a lot of space explaining the hydroxyl-cycle mechanism, there are still many confusing details. In other words, some conclusions can't be supported. Now, some catalyst could achieve high Faradaic efficiency at a wide range of nitrate concentration. Thus, I think the quality of the manuscript can't match the demand of Nature Communication. Some concerns need to be stressed.

1. What is the existent form of the stated OH species? OH- or •OH? It is strange to capture •OH species at a strong reduction condition at -0.8 V vs. RHE (Figs. 5e and f). •OH species are usually considered strong oxidants to be used in the Fenton reaction or in eliminating organic pollutants (DOI: 10.1021/acs.est.1c00230). Besides, it is confusing that the author stressed the confinement of OH species without pointing out the specific component that plays the role of confinement. Nanoconfining is achieved by partial or complete encapsulation or confinement in nanoscope-level space (i.e. nanoscope-limited space), including nanoscope-level channels, two-dimensional interfaces, pores, and cavities (DOI:10.1007/s10311-021-01355-z).

Thank you very much for the valuable comment, and we have carefully considered it based on experiment analysis. In our research, we found that OH species existed in both OH^- and •OH forms, which might serve a separate role during the NO_3RR. Just as the reviewer pointed out, •OH radical was commonly known as an oxidizing free radical used in the Fenton reaction or other environmental applications for organic pollutants elimination. However, it was also generated and observed even in the electrocatalytic reduction process such as CO_2 reduction and O_2 reduction [1-3]. For instance, Mu et al. revealed that the rapid oxidation of Cu catalysts in electrocatalytic CO_2 reduction at negative potential originated from the transient production of •OH radical at room temperature [1]. The emergence of •OH might be ascribed to the co-excitation of factors such as the electrolyte environment, temperature fluctuations and catalyst characteristics, etc [2-3]. As for the

nitrate reduction reaction, we also validated the generation of •OH radical and elucidated the roles of •OH in the OH cycle based on further experiments and characterization:

As for the •OH species, we first repeated EPR measurements to validate the generation of •OH during the nitrate reduction reaction. At open circuit potential (OCP), no signal was detected by DMPO. However, •OH signal was observed after electrocatalysis at a negative potential (-0.8 V vs. RHE) in our reaction system, similar to the observation by Mu et al [1]. It was thought •OH might help to re-oxidate the previously reduced Ni, resulting in potential active metastable $Ni(OH)_2$/Ni state **(Figure 1a, Figure 2)**. For comparison, pure metallic Ni@CF was also prepared and characterized **(Figure 3)**, which indicated no •OH signal was generated either at OCP or at the operating potential in contrast **(Figure 1b)**. This implied the generation of radicals might be related to the intrinsic characteristics catalyst in the electrolyte, which might also have certain effect on the construction of a dynamic $Ni(OH)_2$/Ni interface which was involved in the following OH cycle.

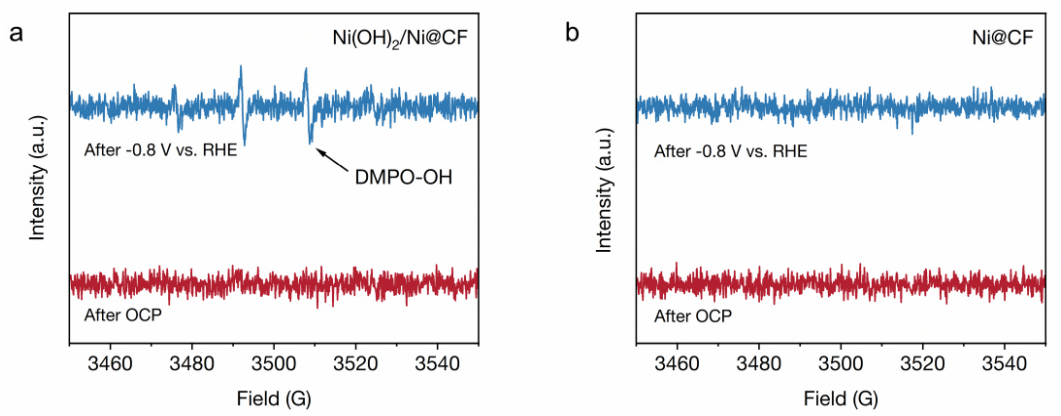

Figure 1. Repeated quasi in-situ EPR spectra of collected electrolyte from NO_3RR using (a) $Ni(OH)_2$/Ni @CF and (b) Ni@CF as electrocatalysts at -0.8 V vs. RHE in 1 M KOH.

[Redacted]

Figure 2. Standard EPR spectrum of DMPO-OH (DOI: 10.3791/54765).

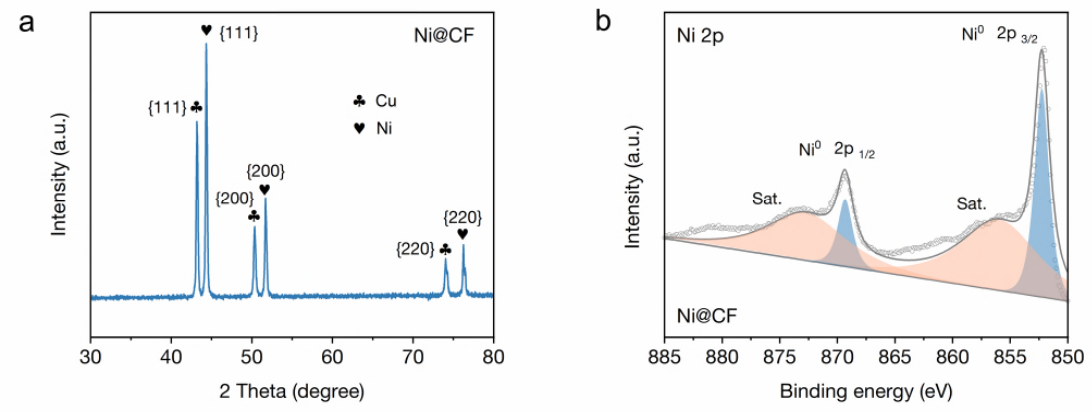

Figure 3 (Fig. S43-44 in SI). Characterization of Ni@CF. **(a)** XRD pattern of Ni@CF. **(b)** XPS Ni 2p spectra of Ni@CF.

The evolution of OH^- was important and worth to trace in this reaction. In addition to the rich OH^- source from the alkaline environment, part of OH^- species involved in hydrogenation of nitrogen-related species and OH cycle was from the electrocatalyst itself. In present work, we tried to track the evolution of OH species, related to the interexchange between catalyst and electrolyte and equilibrium of water dissociation, using isotopically labeled $Ni(OD)_2$/Ni@CF catalyst for the following electrochemical measurements. As shown in **Figure 4a**, we first used H_2O as the electrolyte and $Ni(OD)_2$/Ni@CF catalyst as the cathode for NO_3RR. The in-situ DEMS displayed the signals of m/z=18, 19, and 20, which corresponded to the formation of NH_2D, NHD_2, and ND_3, respectively **(Figure 4b-e)**. Further, we characterized the electrolyte after NO_3RR by ATR-FTIR, and the occurrence of the peak of D-O-D, D-O-H, and -OH confirmed the generation of D_2O/HDO **(Figure 5)**.

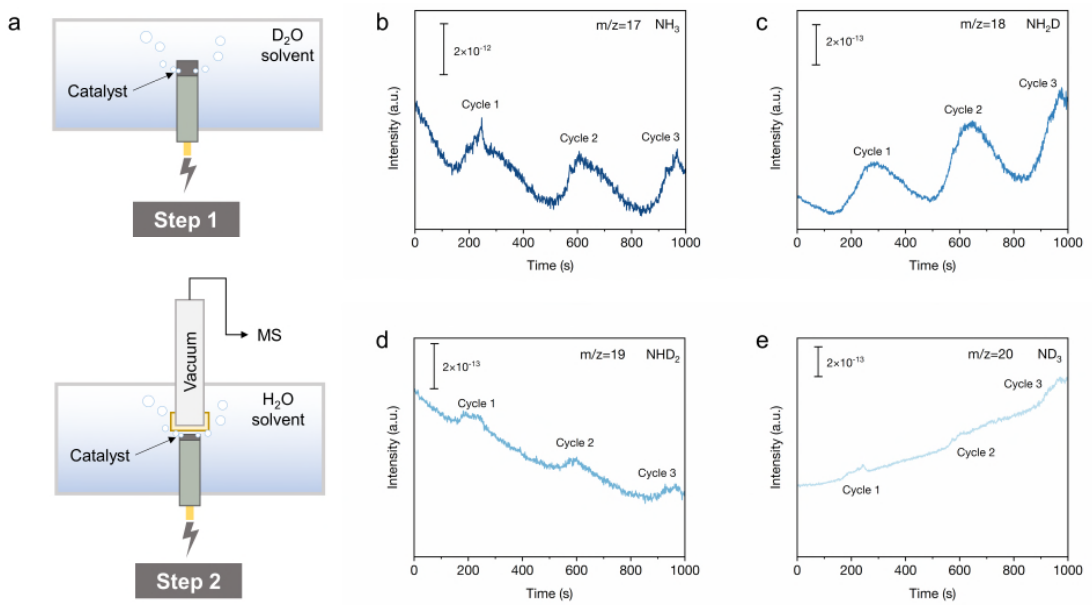

Figure 4 (Fig. S12 in SI). (a) Schematic diagram of the DEMS test. Signals obtained by DEMS during NO_3RR. **(b)** m/z=17, **(c)** m/z=18. **(d)** m/z=19, **(e)** m/z=20.

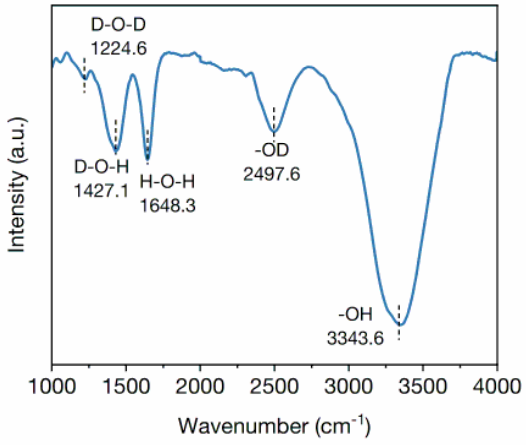

Figure 5. ATR-FTIR spectrum of the electrolyte after in-situ DEMS test.

We further designed serial isotope-labeling experiments **(Figure 6)**. After step I, we refreshed the electrolyte and continued NO_3RR, while almost no D_2O and NH_xD_{3-x} was detected in step II, confirming the depletion of D-containing hydroxyl on the previous catalyst surface. Subsequently, the catalyst was again soaked in D_2O at open circuit potential (OCP) in step III, and the D/H ratio of the electrolyte increased to 0.17. This phenomenon demonstrated that the $Ni(OD)_2$/Ni interface was metastable rather than static, where the metallic Ni readily regenerated into $Ni(OD)_2$ by spontaneously bonding to the hydroxyl group in the solvent. This process was repeated to ensure accuracy and confirm its regularity and reproducibility in step V and VI. Therefore, the $Ni(OD)_2$/Ni@CF interface has a strong interaction with the surface water **(Figure 7).** The de-

hydroxylation effect of the prepared electrocatalyst involved in the formation of surface water, while in-situ generated Ni sites were prone to adsorb OH, thereby activate the surface H_2O and drive H_2O dissociation and the ionization equilibrium of surface water. The obtained H transferred and participated in the hydrogenation of N-species on the electrocatalyst. This whole process might be contributed to a OH cycle mechanism of $Ni(OH)_2$/Ni@CF surface, to promote nitrate electroreduction and inhibiting hydrogen evolution.

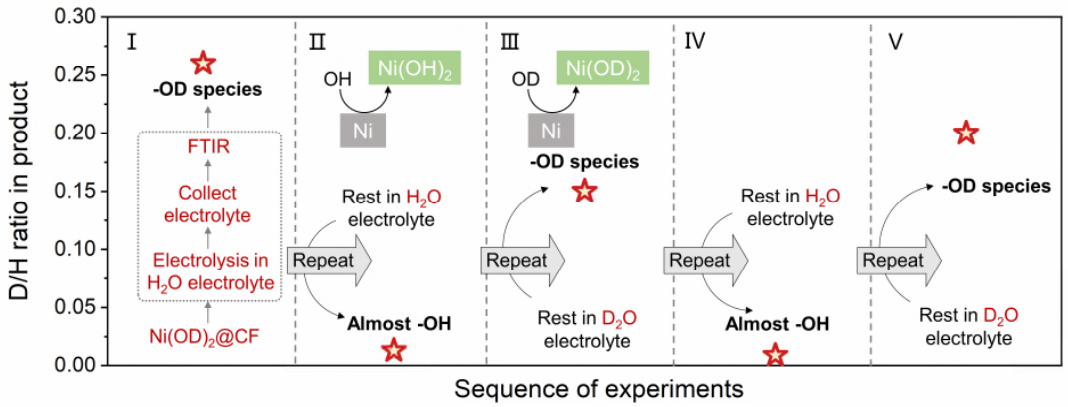

Figure 6 (Fig. S14 in SI). The semi-quantitative FTIR results of the D_2O and H_2O ratio in different operating conditions.

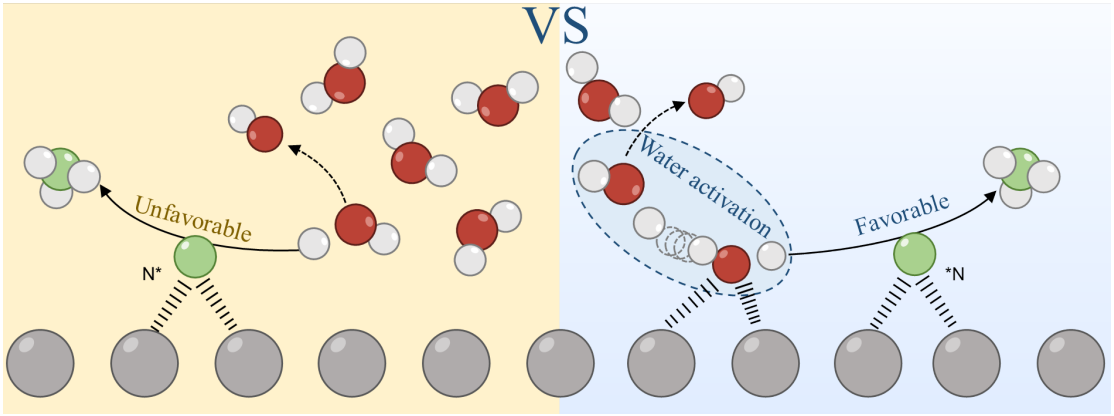

Figure 7. Schematic diagram during NO_3RR process including OH cycle mechanism.

The corresponding discussion has been added in line 153 as follows: *"In-situ differential electrochemical mass spectrometry (DEMS) measurements were further carried out using H/D isotopic labeling to understand the OH evolution process. Firstly, the catalyst was labeled by operating in the electrolyte with H_2O and D_2O solvent, respectively. Then, NO_3RR was performed in the electrolyte with H_2O solvent after thoroughly washing, and the generated volatile products were measured using DEMS (Fig. S12-13)* [28]*. As predicted, $NHxD_{3-x}$ signals (m/z=18, 19, and 20) assigned to NH_2D, NHD_2, and ND_3 was only detected on the catalyst pretreated in D_2O solvent, providing solid evidence to the*

interchange between lattice OH and electrolyte OD during the reaction (Fig. 2b-c) [29]

To further elucidate the role of OH migration as well as the interplay between catalyst surface and electrolyte during NO_3RR, serial isotopic labeling experiments were designed to trace the dynamic interface behavior using Attenuated total reflection Fourier transformed infrared (ATR-FTIR) (Fig. S14). (I) Initially, the $Ni(OD)_2$@CF catalyst prepared via D_2O was employed for NO_3RR with H_2O-based electrolyte. The peak located at 2497.7 cm^{-1} and 3343.6 cm^{-1} was discerned, assigning to D_2O and H_2O species, respectively (Fig. S15). The semi-quantitative ratio of D_2O/H_2O (D/H) determined by FTIR was 0.26, which was also confirmed by Raman spectra (Fig. S16-17). The appearance of D_2O species implied that the interfacial OH from catalyst participated in NO_3RR with water as a medium via the equilibrium of water dissociation."

Previously, we attempted to use 'confinement' to illustrate the potential local-hydroxyl-enrich microenvironment during the reaction. And thank you very much for your suggestion, I have carefully researched the corresponding papers, and find the confinement effect normally be explained as the geometric constraints imposed by nanocavities on objects (zeolites, CNTs, 2D graphene, etc). Although not as the interactions within enclosed spaces, similar interactions between guest molecules and open host surfaces have also been observed. Recent works indicated that metastable nanolayers can maintain a relatively stable state on the open host surface, such as the presence of defect nano-island [4], coordinatively unsaturated sites [5], and self-dispersing oxide [6], etc. These works reported that the interfacial bonds were regulated to create a confinement state on an open surface by manipulating the chemical microenvironment. In our work, the interface OH was co-influenced by **electric field** and the **surface metastable bonding tendency,** resulting in a OH enrichment at the electrode-electrolyte interface.

To avoid ambiguity, the corresponding expression such as 'confinement' has been modified in revised manuscript to avoid any misunderstanding.

[1] S. Mu et al. Hydroxyl radicals dominate reoxidation of oxide-derived Cu in electrochemical CO_2 reduction. *Nat. Commun.* **13**, 3694 (2022).

[2] H. Pan et al. Recent advances in bicarbonate-activated hydrogen peroxide system for water treatment. *Chem. Eng. J.* **408**, 127332 (2021).

[3] J. Noë et al. Evidence for OH Radical Production during Electrocatalysis of Oxygen Reduction on Pt Surfaces: Consequences and Application. *J. Am. Chem. Soc.* **134**, 2835-2841 (2012).

[4] J. Fester, et al. Edge reactivity and water-assisted dissociation on cobalt oxide nanoislands. *Nat. Commun.* **8**, 14169 (2017).

[5] Q. Fu, et al. Interface-Confined Ferrous Centers for Catalytic Oxidation. *Science*. **328**, 1141-1144 (2010).

[6] J. Wang, et al. Confinement-Induced Indium Oxide Nanolayers Formed on Oxide Support for Enhanced CO_2 Hydrogenation Reaction. *J. Am. Chem. Soc*. **146**, 5523–5531 (2024).

2. As the author stated in the manuscript, there are hydroxyl vacancies after NTP treatment, it is recommended the authors compare the content of surface Ni-OH species through XPS analysis (Nat. Mater. 20, 1240–1247 (2021).

Thank you for this valuable suggestion. To gain deeper insights into the impact of non-thermal plasma (NTP) treatment on the catalyst hydroxyl vacancy, we further conducted XPS characterization **(Figure 1)**. After plasma treatment, the Ni 2p peaks exhibited a distribution indicating the presence of both ionic Ni^{2+} (Ni-OH) and metallic Ni^0. Besides, we further investigated the effect of NTP power on the content of surface Ni-OH species. It was observed the ratio of Ni^0:Ni^{2+} increased with the increase of plasma power **(Figure 2)**, suggesting a declining tendency of the concentration of surface Ni-OH species [1].

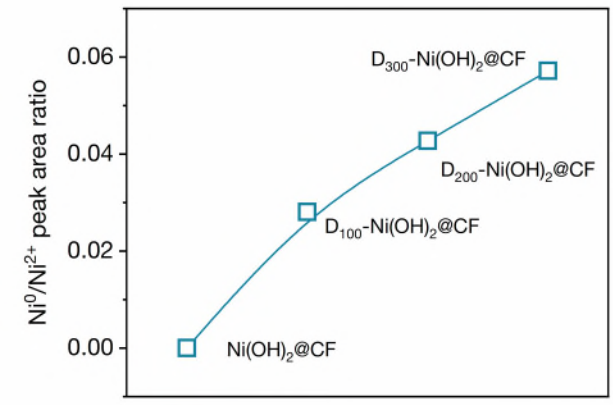

Figure 1 (Fig. S27 in SI). Ni^0/Ni^{2+} ratio obtained by XPS peak area.

Considering the errors associated with XPS peak fitting, we also measured the peak positions, and the increasing offset (0.15 eV→0.24 eV→0.32 eV) further corroborated the reduction in surface Ni-OH species [2].

We also supplemented both references (*Nat. Mater. 20, 1240–1247, 2021; J. Phy: Condens Matter*. 4, 7973-7978,1992) in citations [34] and [35] within the manuscript. The corresponding

discussion has been made in line 232 as follows: *"Correspondingly, the ratio of Ni^0:Ni^{2+} increased from 0.01 to 0.06, with the monotonic shift of the Ni 2p peak position from 0.15 to 0.32 eV, confirming the reducing of surface Ni-OH species via NTP treatment (Fig. S25-27)* [34, 35]*."*

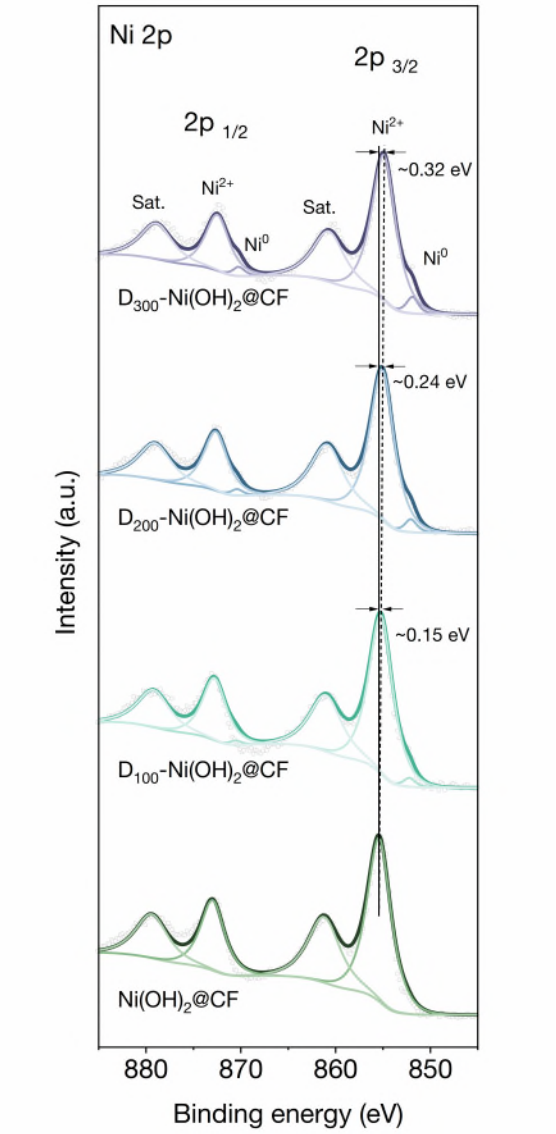

Figure 2 (Fig. S28 in SI). Ni 2p XPS spectra of $Ni(OH)_2$@CF, D_{100}-$Ni(OH)_2$@CF, D_{200}-$Ni(OH)_2$@CF, and D_{300}-$Ni(OH)_2$@CF, respectively (100, 200, 300 represented the power of NTP).

[1] S. Li et al. Oxygen-evolving catalytic atoms on metal carbides. *Nat. Mater.* **20**, 1240-1247 (2021).

[2] S. Uhlenbrock, et al. The influence of defects on the Ni 2p and O 1s XPS of NiO. *J. Phy: Condens Matter*. 4, 7973-7978 (1992).

3. It would be better if the authors provided the raw data of the in situ Raman test in supplementary information. Notably, for $Ni(OH)_2$/Ni@CF, the surface is composed of Ni and $Ni(OH)_2$. For the

defect-rich D-Ni(OH) /Ni@CF, the Raman peaks of Ni-OH vanished completely (Fig. 5C). At this time, does the proposed hydroxyl-cycle mechanism work? Then, The name of D-Ni(OH)$_2$/Ni@CF used in the manuscript indicated the formation of a special structure. The author should provide the XRD data to support their idea.

Thanks very much for your suggestion. Firstly, we supplemented the raw data of the in-situ Raman with the form of the line graph as follows **(Figure 1-2)**:

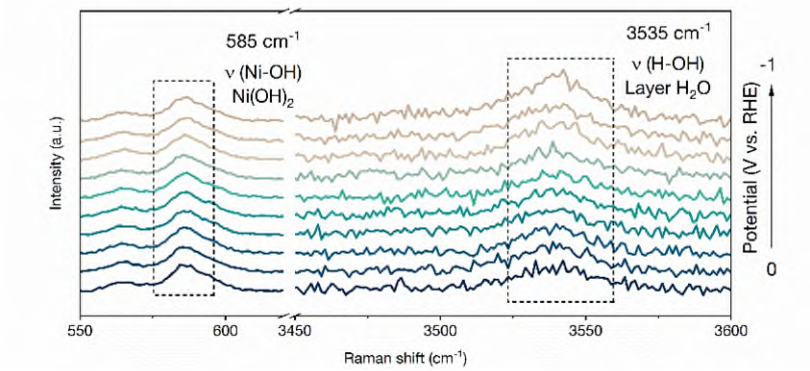

Figure 1 (Fig. S11 in SI). Raw data of in situ electrochemical Raman spectra of Ni(OH)$_2$/Ni@CF from 0 to -1.0 V vs. RHE in the electrolyte with 0.1 M KNO$_3$ + 1 M KOH.

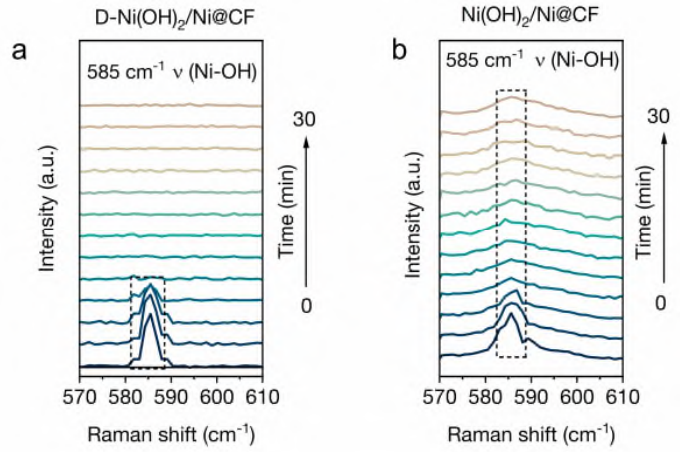

Figure 2 (Fig. S35 in SI). Raw data of in situ electrochemical Raman spectra at -0.8 V vs. RHE of **(a)** D-Ni(OH)$_2$/Ni@CF and **(b)** Ni(OH)$_2$/Ni@CF with a time scale of 0~30 min.

Secondly, given the high surface sensitivity of the Raman signal, it focused on probing structural details exclusively at the electrode-electrolyte interface. To comprehensively elucidate the catalyst structure, we complemented XRD characterization for the catalyst after electrocatalysis **(Figure 4)**. Remarkably, the persistence of the Ni(OH)$_2$ in XRD patterns indicated the maintaining of the Ni(OH)$_2$ within the catalyst bulk. Moreover, the previously observed *OH radicals might also reoxidate the surface, and it was speculated the surface existed certain dynamics equilibrium.

Furthermore, the OH signal on D-Ni(OH)2/Ni@CF surface through in-situ FTIR further confirmed the presence of adsorbed OH involved the surface OH cycle **(Figure 3)**. The isotopic labelling via DEMS implied the continuous interchange between catalyst and electrolyte.

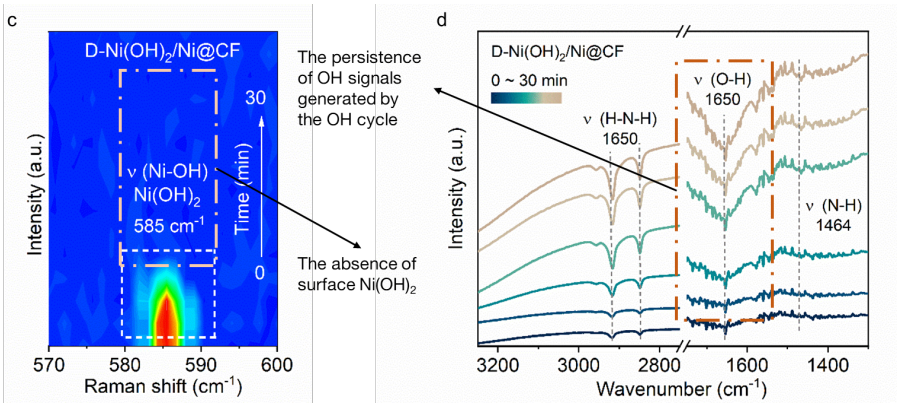

Figure 3 (Fig. 4c-d in manuscript). (c) In situ electrochemical Raman spectra at -0.8 V vs. RHE of D-Ni(OH)2/Ni@CF with a time scale of 0~30 min. **(d)** In situ electrochemical FTIR spectra at -0.8 V vs. RHE of D-Ni(OH)2/Ni@CF with a time scale of 0~30 min.

Finally, we supplemented the XRD pattern of D-Ni(OH)2/Ni@CF **(Figure 3)**. Apart from the signal of the Cu substrate, the catalyst primarily comprised of mixed phases of Ni and Ni(OH)2 **(Figure 4a)**. We further conducted the positron annihilation lifetime spectroscopy (PALS) test to demonstrate the special structure of D-Ni(OH)2/Ni@CF, which cannot be discerned in XRD pattern **(Figure 4b)**. The extension of the defect relaxation time τ_1 from 114 to 128 ps illustrated the atomic scale hydroxyl vacancy appears on D-Ni(OH)2/Ni@CF after plasma treatment. We also supplemented the corresponding discussion in line 217 as follows: *"As expected, HR-TEM images showed the co-existence of lattice fringe of 0.267 nm and 0.203 nm, corresponding to the {100} facet of Ni(OH)2 and {111} facet of Ni in D-Ni(OH)2/Ni@CF after NO3RR, consistent with the XRD pattern (Fig. 4a-b, Fig. S24)"*

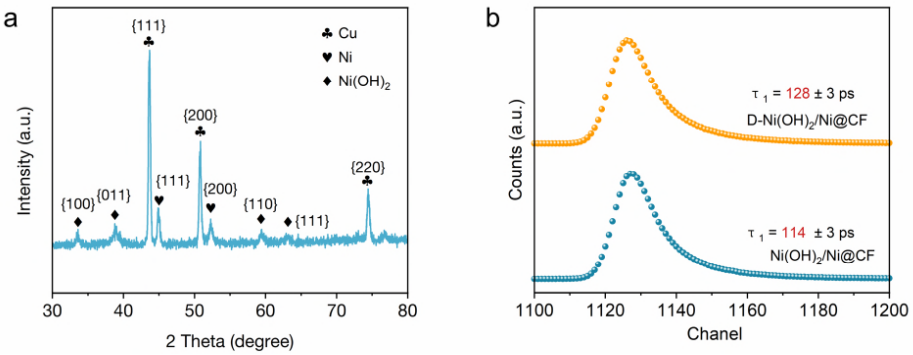

Figure 4. Characterization of D-Ni(OH)2/Ni@CF. **(a)** XRD pattern of D-Ni(OH)2/Ni@CF **(Fig. S25 in SI)**. **(b)** Positron annihilation lifetime spectroscopy (PALS) spectra of Ni(OH)2/Ni@CF and D-Ni(OH)2/Ni@CF **(Fig. 4c in manuscript).**

4. In Figure 3b, the authors used FTIR to determine the ratio of deuterium ammonia to ammonia (D/H), but no related FTIR spectra were supplemented either in the main text or in the supplementary information. Besides, considering the complexity of the IR spectrum, online DEMS was more suitable for studying the process of surface OH desorption → limited OH diffusion → OH participation in the hydrogenation (Nat Catal 4, 1012–1023 (2021); DOI:10.1002/smll.202303249).

Thanks very much for your suggestion. We supplemented the ATR-FTIR data in the supplementary information **(Figure 1-3)**.

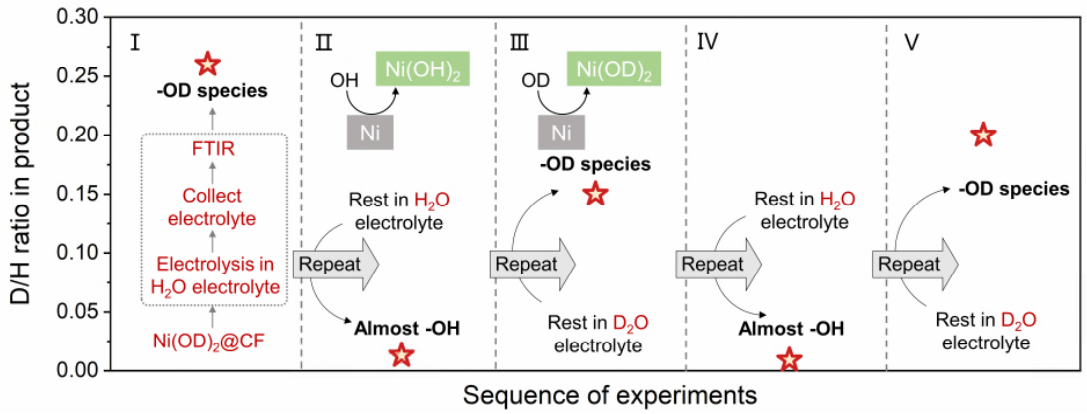

Figure 1 (Fig. S14 in SI). The semi-quantitative FTIR results of the D2O and H2O ratio in different operating conditions.

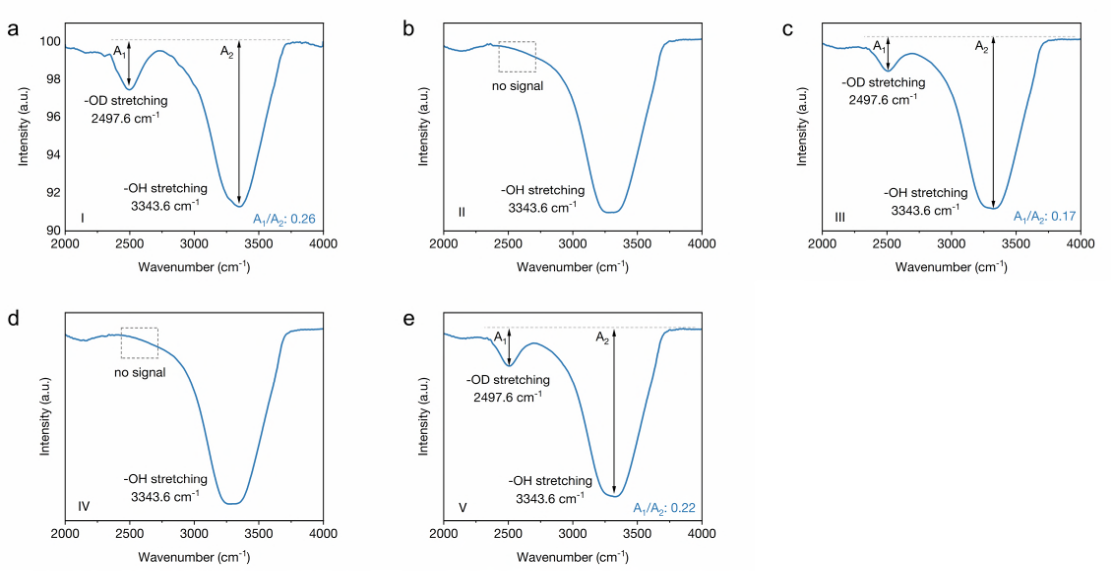

Figure 2 (Fig. S15 in SI). ATR-FTIR spectrum from 2000 to 4000 cm^{-1} of the electrolyte corresponding to experiment I to V.

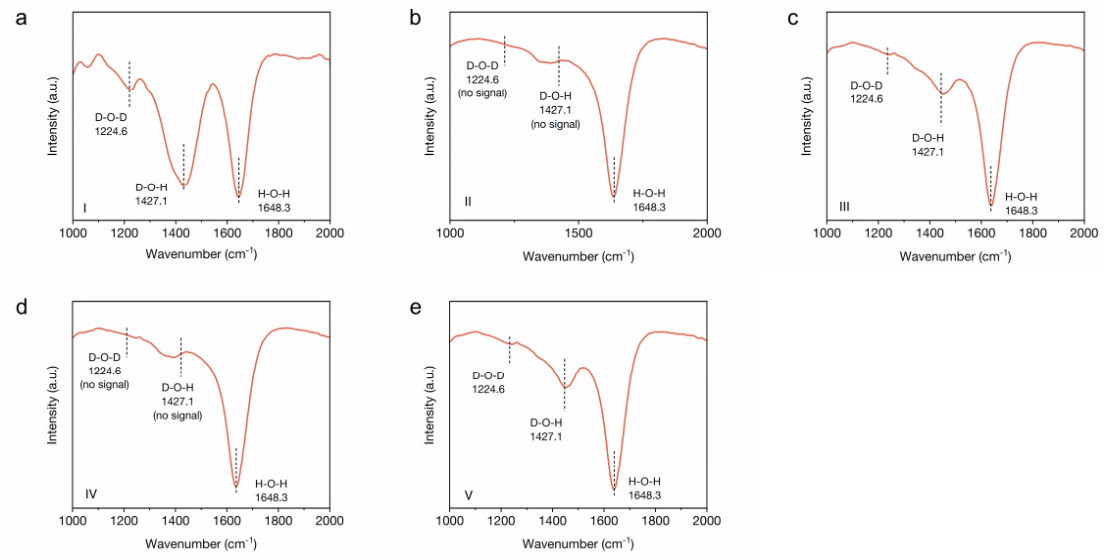

Figure 3. ATR-FTIR spectrum from 1000 to 2000 cm^{-1} of the electrolyte corresponding to experiment I to V.

The FTIR peak observed at ~2497.6 cm^{-1} should be ascribed to D_2O/HDO species rather than NH_xD_{3-x} after careful consideration [1-2], given that the N-H signal was considerably weaker compared to H-OH. Nevertheless, the proposed OH cycle still holds with OH participation in NO_3RR with H_2O as a medium, therefore the appearance of D_2O/HDO signal attributed to the de-hydroxylation of the electrocatalyst and then involved with the equilibrium of water dissociation. Thus, we further investigated performed the measurements by DEMS for NH_xD_{3-x} species and ATR-FTIR for D_2O species.

Thanks very much to propose on-line DEMS, which offered precise measurement for the intermediate products during electrochemical reactions. Although OH cannot be directly detected by DEMS, we can isotopically label the surface OH (by using OD), enabling us to track its involvement during the reaction as follows:

To further verify the evolution of OH during NO_3RR, in situ DEMS measurements was performed with H/D isotope labeling [1-2]. Similarly, the $Ni(OH)_2$/Ni@CF catalyst was firstly labeled via electrocatalysis in the electrolyte with H_2O and D_2O as the solvent, respectively **(Figure 4a, Figure 5a)**. Second, NO_3RR was performed in the electrolyte with H_2O as the solvent after thoroughly washing of prepared catalyst. The generated gas during the reaction was measured using DEMS. Due to the exchange between the lattice OH in the catalyst and OD in solution during the first step, $Ni(OD)_2$/Ni@CF catalyst containing OD species was created. Thus, NH_xD_{3-x} product was expected to be produced in the second step. As expected, NH_xD_{3-x} signals (m/z=18, 19, 20) was observed **(Figure 4b-e)**, directly providing the solid experimental evidence to confirm the origin of OH from $Ni(OH)_2$/Ni@CF surface and its involvement of OH cycle, consistent with the semi-quantitative ATR-FTIR results based on isotope labeling **(Figure 2, Figure 3)**. However, no NH_xD_{3-x} species were observed on the catalyst pretreated with H_2O solvent, excluding signal interference caused by other contaminants **(Figure 5b-c)**.

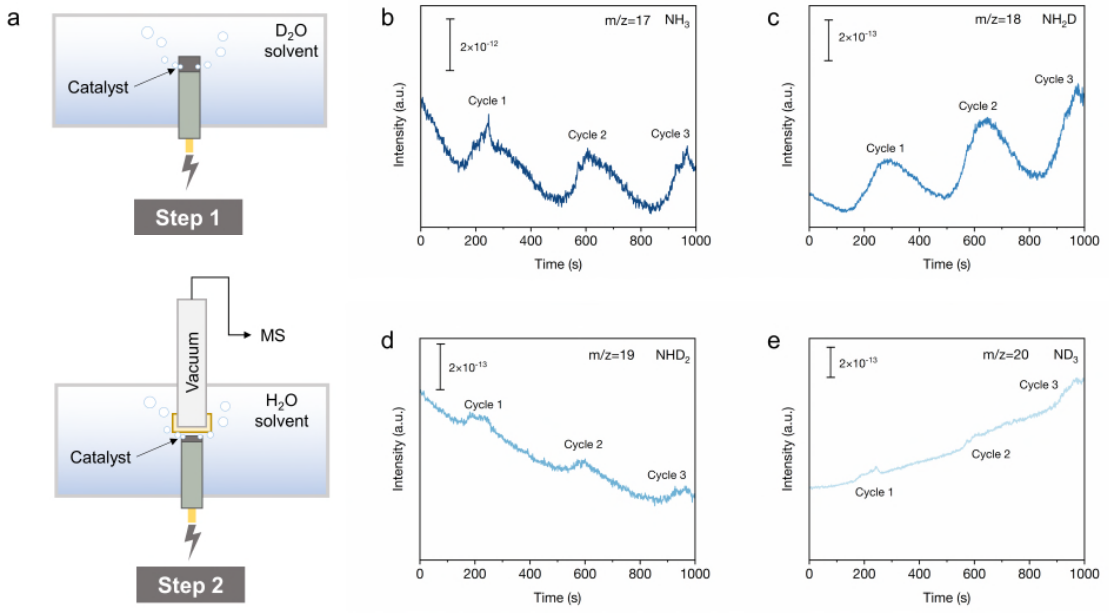

Figure 4 (Fig. S12 in SI). (a) Schematic diagram of the DEMS test with D_2O solvent pretreatment. Signals obtained by DEMS during NO_3RR. **(b)** m/z=17, **(c)** m/z=18. **(d)** m/z=19, **(e)** m/z=20.

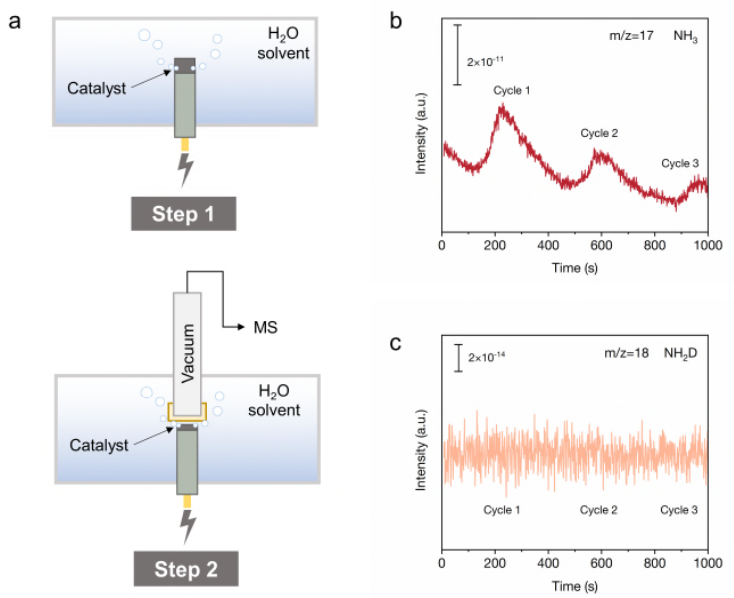

Figure 5 (Fig. 13 in SI). (a) Schematic diagram of the DEMS test with H_2O solvent pretreatment. Signals obtained by DEMS during NO_3RR. **(b)** m/z=17, **(c)** m/z=18.

Finally, we supplemented the corresponding discussion in line 153 as follows: *"In-situ differential electrochemical mass spectrometry (DEMS) measurements were further carried out using H/D isotopic labeling to understand the OH evolution process. Firstly, the catalyst was labeled by operating in the electrolyte with H_2O and D_2O solvent, respectively. Then, NO_3RR was performed in the electrolyte with H_2O solvent after thoroughly washing, and the generated volatile products were measured using DEMS (Fig. S12-13)* [28]*. As predicted, $NHxD_{3-x}$ signals (m/z=18, 19, and 20) assigned to NH_2D, NHD_2, and ND_3 was only detected on the catalyst pretreated in D_2O solvent, providing solid evidence to the interchange between lattice OH and electrolyte OD during the reaction (Fig. 2b-c)* [29]*.*

To further elucidate the role of OH migration and key intermediates during NH_3 synthesis, serial isotopic labeling experiments were designed to trace the dynamic interface behavior using Attenuated total reflection Fourier transformed infrared (ATR-FTIR) (Fig. S14). (I) Initially, the $Ni(OD)_2$@CF catalyst prepared via D_2O was employed for NO_3RR with H_2O-based electrolyte. The peak located at 2497.7 cm^{-1} and 3343.6 cm^{-1} was discerned, assigning to D_2O and H_2O species, respectively (Fig. S15). The semi-quantitative ratio of D_2O/H_2O (D/H) determined by FTIR was 0.26, which was also confirmed by Raman spectra (Fig. S16-17). The appearance of D_2O species implied that the interfacial OH from catalyst participated in NO_3RR with water as a medium via the equilibrium of water dissociation."

[1] C. Lin et al. In-situ reconstructed Ru atom array on α-MnO_2 with enhanced performance for acidic water oxidation. *Nat. Catal.* **4**, 1012-1023 (2021).

[2] X. Tan et al. Electrochemical Etching Switches Electrocatalytic Oxygen Evolution Pathway of $IrO_x/Y_2O_3$from Adsorbate Evolution Mechanism to Lattice-Oxygen-Mediated Mechanism. *Small*. **19**, 2303249 (2023).

5. The assignment of Raman peaks in Fig S11 needs to be reconsidered. The peak range from 3200 to 3600 cm^{-1} is usually related to H_2O (Nature Protocols 2023, 18, 883-901; Nature 2021, 600, 81-85). In other words, it is recommended to provide the Raman spectra of standard NH_3, ND_3, and H_2O to support the peak assignment.

Thanks very much for your suggestion and it is our mistake. We have carefully checked that the peaks in both spectra should be attributed to D_2O. To provide a rigorous demonstration, we conducted Raman tests on standard samples of D_2O, H_2O, and a mixed sample of D_2O and H_2O. The results indicated that the newly observed Raman peak at ~2582 cm^{-1} should be attributed to the D_2O species **(Figure 1)**. And we have corrected it in our revised manuscript.

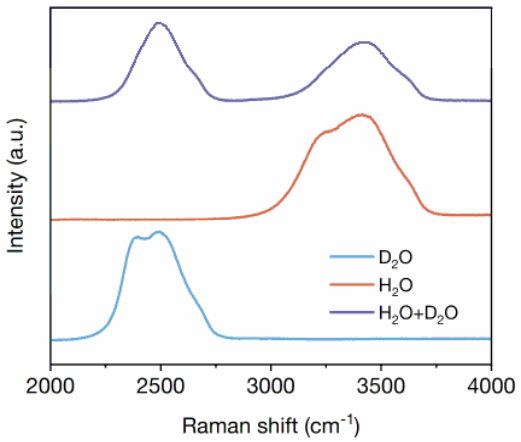

Figure 1 (Fig. S16 in SI). Raman spectra of standard **(a)** D_2O, **(b)** H_2O, and **(c)** a mixed sample of D_2O and H_2O.

6. After NTP treatment, the ECSA of D-$Ni(OH)_2$/Ni@CF increased a lot. The introduction of plasma treatment may introduce holes in the catalysts' surface and enlarge the specific surface area. After normalizing to the ECSA, would D-$Ni(OH)_2$/Ni@CF still own the better activity?

Thanks very much for your question. D-$Ni(OH)_2$/Ni@CF exhibited a larger ECSA than $Ni(OH)_2$/Ni@CF, but might not be directly attributed to surface defects introduced by plasma treatment. We supplemented ECSA measurements immediately using the freshly prepared catalyst,

which reflected the intrinsic activity of the catalyst **(Figure 1)**. The comparable ECSA values for D-Ni(OH)$_2$/Ni@CF (57.3 mF cm^{-2}) and Ni(OH)$_2$/Ni@CF (51.9 mF cm^{-2}) immediately after the catalyst preparation indicated that the surface holes caused by plasma were not sufficient to greatly change the catalytic activity. Further, we compared the activity of D-Ni(OH)$_2$/Ni@CF and Ni(OH)$_2$/Ni@CF by ECSA normalizing:

$$j_{\text{ECSA normalized D-Ni(OH)2/Ni@CF}} = j_{\text{D-Ni(OH)2/Ni@CF}} * \text{ECSA}_{\text{Ni(OH)2/Ni@CF}} / \text{ECSA}_{\text{D-Ni(OH)2/Ni@CF}} \quad (1)$$

The greater normalized current density on D-Ni(OH)$_2$/Ni@CF than Ni(OH)$_2$/Ni@CF also demonstrated the better activity of D-Ni(OH)$_2$/Ni@CF **(Figure 2)**.

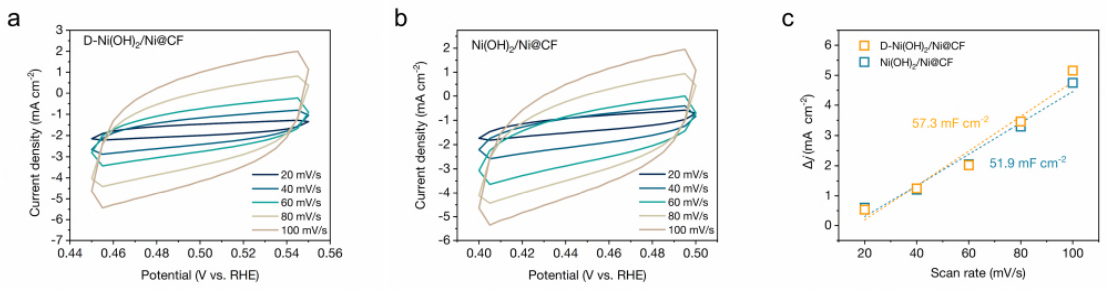

Figure 1 (Fig. S28-29 in SI). CV curves immediately after catalyst preparation in the non-faradaic area with different scan rates (20 mV/s, 40 mV/s, 60 mV/s, 80 mV/s, and 100 mV/s) of **(a)** D-Ni(OH)$_2$/Ni@CF and **(b)** Ni(OH)$_2$/Ni@CF. **(c)** The double layer capacitance (Cdl) of Ni(OH)$_2$/Ni@CF and D-Ni(OH)$_2$/Ni@CF immediately after catalyst preparation calculated by CV curves.

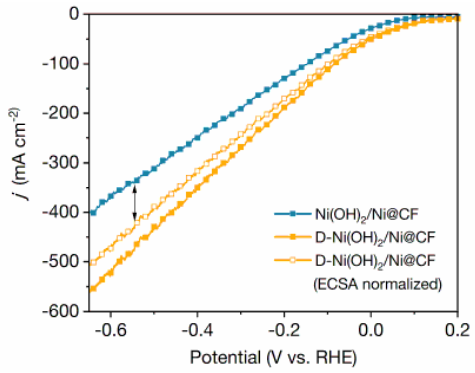

Figure 2 (Fig. 3g in manuscript). Polarization curves measured by linear sweep voltammetry (LSV) from 0.2 V vs. RHE to -0.65 V vs. RHE of Ni(OH)$_2$/Ni@CF, D-Ni(OH)$_2$/Ni@CF, and ECSA normalized D-Ni(OH)$_2$/Ni@CF. ($j_{\text{ECSA normalized D-Ni(OH)2/Ni@CF}} = j_{\text{D-Ni(OH)2/Ni@CF}} * \text{ECSA}_{\text{Ni(OH)2/Ni@CF}} / \text{ECSA}_{\text{D-Ni(OH)2/Ni@CF}}$)

In fact, we also measured ECSA after a series of electrochemical measurements **(Figure 3)**. The surface of the D-Ni(OH)$_2$/Ni@CF catalyst has exhibited more metallic Ni sites due to enhanced OH cycle than Ni(OH)$_2$/Ni@CF, which can be thoroughly validated by previous in-situ Raman

spectroscopy and in situ FTIR. Thus, this larger ECSA on D-Ni(OH)2/Ni@CF was attributed to the fast OH cycle instead of surface defect.

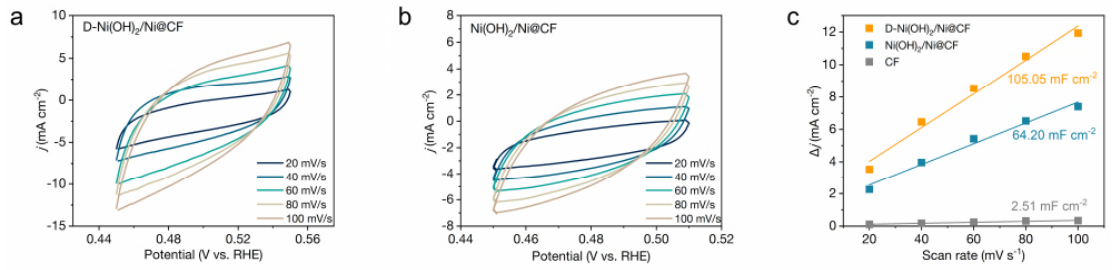

Figure 3 (Fig. S33-34 in SI). CV curves (after electrocatalysis) in the non-faradaic area with different scan rates (20 mV/s, 40 mV/s, 60 mV/s, 80 mV/s, and 100 mV/s) of **(a)** D-Ni(OH)2/Ni@CF and **(b)** Ni(OH)2/Ni@CF. **(c)** The double layer capacitance (Cdl) of Ni(OH)2/Ni@CF and D-Ni(OH)2/Ni@CF after electrocatalysis calculated by CV curves.

We also supplemented the corresponding discussion in line 242 as follows: *"We initially evaluated the ESCA of the freshly prepared catalyst for comparison, revealing the comparable C_{dl} values for D-Ni(OH)2/Ni@CF (57.3 mF cm^{-2}) and Ni(OH)2/Ni@CF (51.9 mF cm^{-2}) (Fig. S28-29). Polarization curves exhibited a substantially lower overpotential and larger current density of D-Ni(OH)2/Ni@CF (-562.6 mA cm^{-2}) compared to CF (157.63 mA cm^{-2}) and Ni(OH)2/Ni (400.45 mA cm^{-2}), indicating accelerated kinetics of NO_3RR electrochemical reaction on activated interface (Fig. 3g). After normalizing the current density on D-Ni(OH)2/Ni@CF to that of Ni(OH)2/Ni@CF by ECSA, the catalytic activity remained superior (503.96 mA cm^{-2}), excluding the effect from the surface roughness modification by NTP. Through long-term electrosynthesis of NH_3, the ECSA on D-Ni(OH)2/Ni@CF (105.05 mF cm^{-2}) increased more significantly than that of Ni(OH)2/Ni@CF (64.20 mF cm^{-2}), reflected the faster surface evolution on the activated dynamic interface with more active sites (Fig. S33-34)"*

7. The experimental details of the in situ experiment need to be supplemented. For example, if the experimental details of EPR experiments were not controlled, the obtained spectra cannot be used to compare the number of defects or the number of generated ·OH.

Thanks for your suggestion. We supplemented following content in 4.3 In situ experiments (line 414), including other characterizations like in-situ DEMS: *"In-situ EPR measurements were employed to capture the formation of free radicals during electrochemical reactions (EPR, Bruker ESRA-300). The NO_3RR was conducted in a 10 mL H-cell with 1 M KOH + 0.1 M KNO_3 electrolyte, using a membrane*

for separation. A Pt plate, an Ag/AgCl electrode filled with 3 M KCl, and the catalyst served as the counter electrode, reference electrode, and working electrode, respectively. After 300 s of potentiostatic operation at -0.8 V vs. RHE, 0.5 mL of diluted DMPO was introduced into the electrolyte. Sample analysis was performed after thorough stirring for 100 s. In-situ DEMS measurements were conducted by using QAS100 instrument (Linglu China) to capture volatile intermediates and products. A catalyst-coated electrode, Pt wire, and Ag/AgCl electrode were employed as the working electrode, counter electrode, and reference electrode, respectively. Volatile products were transported through a PTFE membrane via a vacuum pump to the mass spectrometer. The DEMS primarily targeted products with mass-to-charge ratios (m/z) of 17, 18, 19, and 20 (corresponding to NH_3, NH_2D, NHD_2, and ND_3, respectively). The DEMS test comprised two steps: firstly, the two groups of catalysts underwent NO_3RR in D_2O and H_2O solvents, respectively. Subsequently, the catalysts tested in H_2O solvent using LSV method for working cycle after thoroughly rinsed."

Thank you very much for these valuable suggestions to help us get insight into the mechanism. We have completely updated the manuscript. Sincerely thank you for improving the quality of this manuscript!

Reviewer #2 (Remarks to the Author):

This manuscript reports an intriguing effect of electrocatalyst-electrolyte interaction on ammonia synthesis. With $Ni(OH)_2$ as the model electrocatalyst, OH cycle was proposed to be involved in the hydrogeneration process of nitrogen species, which is well backed-up by the in-situ characterization and isotope-labeling experiments. The manuscript should be publishable after the following issues been addressed.

1. The authors claimed that the $Ni(OH)_2$ reconstructed into Ni at ~-2.3 V vs. RHE in Figure 3c. However, the working potential was set as 0~-1.0 V vs. RHE in all the subsequent electrochemical experiments. Please comment.

Thanks very much for your question. Theoretical calculations often overlook several influential factors (electric field, solvation effect, pH value, etc), leading to significant discrepancies between theoretical predictions and experimental results. The phase transition of $Ni(OH)_2$ occurred around -2.3 V vs. RHE in our calculations, whereas experimental observations indicated this transition at approximately 0~-1 V vs. RHE. While there existed disparities in the absolute values between the two results, our primary objective was to demonstrate the propensity of $Ni(OH)_2$ to undergo transformation into Ni at specific negative potentials. This assertion was fully corroborated by both experimental findings and theoretical calculations.

2. The author substantiated the identification of hydroxyl vacancy sites on the catalyst surface through the application of positron annihilation lifetime spectroscopy (PALS) as depicted in Figure 4c. They asserted that the defect relaxation time (τ1) within the range of 114 to 128 ps signifies the emergence of vacancies. Please elaborate or offer more related references. What is τ1?

We thank the reviewer for this question, and it is helpful for the readers to understand the experiments. Positron annihilation lifetime spectroscopy (PALS) injected a positron into a material and measuring the time it takes for the positron to annihilate with one of the electrons in the material [1]. The lifetime of the positron could be calculated as followed (equation 1):

$$N(t) = \sum_i I_i/\tau_i \exp(-t/\tau_i) \quad (1)$$

Where the different vacancy according to the positron annihilation lifetime (τ1, τ1, etc.) [2]. The shortest lifetime (τ1) reflected the annihilation of positrons at small size defects such as oxygen/hydroxyl vacancies [3].

Thus, we have supplemented the above references in the manuscript (Ref 36-38 in manuscript), and added the corresponding methods in line 390 as follows: "*The positron annihilation lifetime spectroscopy (PALS) was measured via the apparatus DPLS3000. The lifetime of the positron could be calculated as followed:* $N(t) = \sum_i I_i/\tau_i \exp(-t/\tau_i)$ *[39-41] (1)*"

[1] F. Tuomisto, et al. Defect identification in semiconductors with positron annihilation: experiment and theory. *Rev. Mod. Phys.* **85**, 1583 (2013).

[2] M. Guan, et al. Vacancy associates promoting solar-driven photocatalytic activity of ultrathin bismuth oxychloride nanosheets. *J. Am. Chem. Soc.* **135**, 10411-10417 (2013).

[3] K. Zhu, et al. Defect engineering on V_2O_3 cathode for long-cycling aqueous zinc metal batteries. *Nat Common.* **12**, 6878 (2021).

3. The XRD patterns of the electrocatalysts were shown in Figure S3-4 to characterize the phase composition of the catalyst. However, conspicuous peaks corresponding to Cu appeared in the XRD patterns. Can the authors elucidate the cause of this observation? Additionally, whether the Cu forms additional active sites? Does Cu impact on the overall performance of the catalyst.

Thanks very much for your question. Our catalyst utilized the Cu foam as the catalyst substrate due to the excellent electrical conductivity and stable structure. Given that XRD characterization revealed information about the bulk phase structure, a series of peaks corresponding to Cu species become evident in the XRD patterns. We supplemented an experiment, and the result revealed that the NH_3 synthesis activity on Cu foam was notably low **(Figure 1)**.

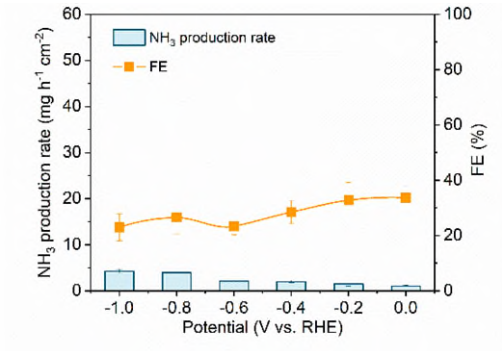

Figure 1 (Fig. S42 in SI). NH_3 production rate and FE of Cu foam (CF) at the potential range from 0.0 to -1.0 V vs. RHE.

Further, we added the characterization. The catalyst surface was stripped and characterized to confirm whether the Ni species was affected by the incorporation of Cu elements. The results from ICP **(Table 1)** and XPS **(Figure 2)** indicated the absence of Cu species on the catalyst surface, suggesting that the influence of the Cu substrate on catalytic activity was limited. We have supplemented the corresponding discussion in line 105 as follows: *"Besides, the prepared catalyst was stripped and characterized independently via X-ray photoelectron spectroscopy (XPS) and inductively coupled plasma optical emission spectrometer (ICP), which confirmed the absence of Cu on the catalyst surface and excluded the potential influence of Cu on enhanced reaction activity (Table. S1, Fig. S5)"*

Table 1 (Table. S1 in SI). ICP-OES results of the surface catalyst after electrocatalysis (ND: not detected).

Element	C_0 (mg/L)
Ni	6.641
Cu	ND
Co	ND
Fe	ND

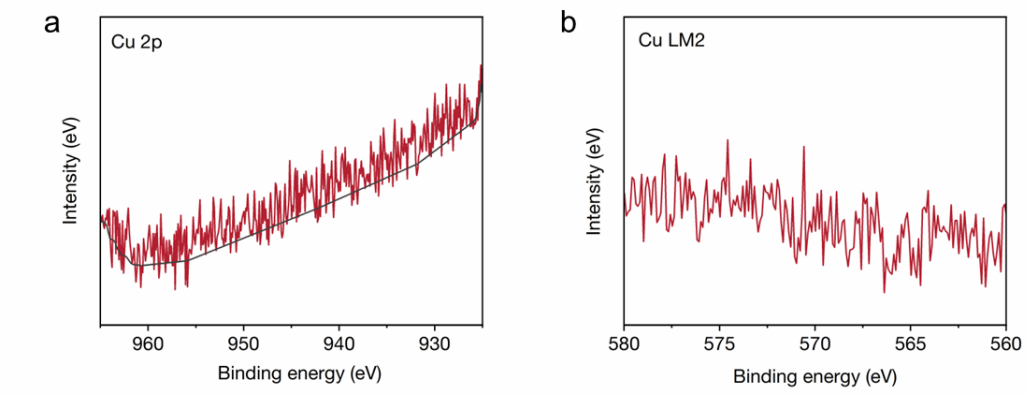

Figure 2 (Fig. S5 in SI). XPS spectra of the surface catalyst after electrocatalysis. **(a)** Cu 2p spectra. **(b)** Cu LM2 spectra.

4. In situ Raman spectroscopy was used to characterize the valence state and phase of the catalyst surface. However, the description of the in-situ Raman method is missing. In addition, the authors did not describe the experimental methods of in situ FTIR and EPR, neither.

Thanks for very much your suggestion. We added more information about in-situ characterization (Raman, FTIR, EPR, and DEMS) in "4.3 In situ experiments" (line 414) as follows: *"In situ EPR measurements were employed to capture the formation of free radicals during electrochemical reactions (EPR, Bruker ESRA-300). The NO_3RR was conducted in a 10 mL H-cell with 1 M KOH + 0.1 M KNO_3 electrolyte, using a membrane for separation. A Pt plate, an Ag/AgCl electrode filled with 3 M KCl, and the catalyst served as the counter electrode, reference electrode, and working electrode, respectively. After 300 s of potentiostatic operation at -0.8 V vs. RHE, 0.5 mL of diluted DMPO was introduced into the electrolyte. Sample analysis was performed after thorough stirring for 100 s. In situ FTIR spectrums were obtained to determine the surface absorption species on catalyst surface (Thermo Fisher, Nicolet iS50) The catalyst was stripped from the CF and processed into an ink for deposition onto a glassy carbon electrode, followed by drying to form the working electrode. In the three-*

electrode system, Pt wire and Ag/AgCl (3 M KCl) electrode were utilized as the counter and reference electrodes, respectively. FTIR data were recorded in reflection mode with a spectral resolution of 2 cm^{-1}. Before data acquisition, the background of the working electrode was recorded in the open circuit potential. The working electrode was maintained at -0.8 V vs. RHE during NO_3RR. In-situ DEMS measurements were conducted by using QAS100 instrument (Linglu China) to capture volatile intermediates and products. A catalyst-coated electrode, Pt wire, and Ag/AgCl electrode were employed as the working electrode, counter electrode, and reference electrode, respectively. Volatile products were transported through a PTFE membrane via a vacuum pump to the mass spectrometer. The DEMS primarily targeted products with mass-to-charge ratios (m/z) of 17, 18, 19, and 20 (corresponding to NH_3, NH_2D, NHD_2, and ND_3, respectively). The DEMS test comprised two steps: firstly, the two groups of catalysts underwent NO_3RR in D_2O and H_2O solvents, respectively. Subsequently, the catalysts tested in H_2O solvent using LSV method for working cycle after thoroughly rinsed."

5. The authors mentioned COHP calculation in the manuscript, but there was no relevant content in the discussion of the results.

Thanks for your suggestion to improve the quality of this manuscript. We are very sorry for the misleading. We employed crystal orbital Hamilton population (COHP) calculations to assess the adsorption capabilities of NO_3^- on different catalytic surfaces. The results revealed that the chemical bond between Ni and the O atom in nitrate on the catalyst surface was notably stronger (ICOHP=-1.81) compared to $Ni(OH)_2$ (ICOHP=-0.61), indicating superior adsorption capacity on the $Ni(OH)_2$/Ni surface **(Figure 1)**.

Thus, we added the discussion of COHP in line 188 as follows: *"Consistently, the energy barrier of the potential-determined step (PDS) on $Ni(OH)_2$/Ni (0.48 eV) was lower than that of $Ni(OH)_2$ (1.40 eV) (Fig. S18-20, Table S3), and the crystal orbital Hamilton population (COHP) proved the better adsorption capacity for NO_3^- on $Ni(OH)_2$/Ni (Fig. S21), revealing the genuine active site originated from $Ni(OH)_2$/Ni surface."*

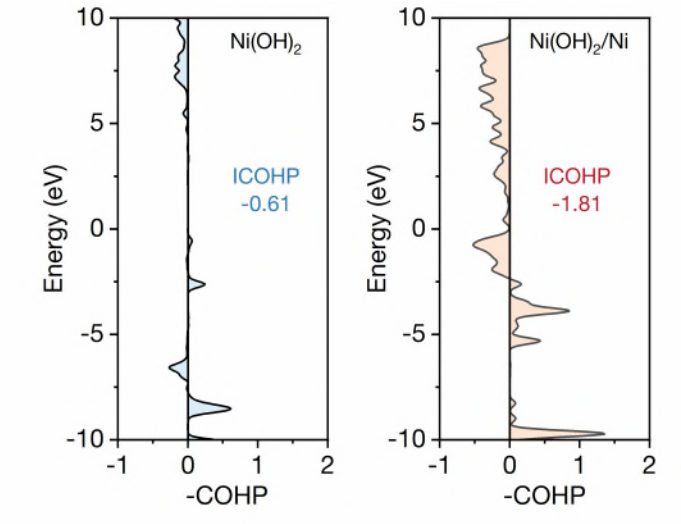

Figure 1 (Fig. S21 in SI). COHP of the bond between O atom of nitrate and catalyst surface on $Ni(OH)_2$ and $Ni(OH)_2/Ni$.

6. HER is perhaps the most important competitive reaction of NO_3RR in aqueous environment, and the activity of D-$Ni(OH)_2$/Ni@CF and $Ni(OH)_2$/Ni@CF for HER reaction needs to be demonstrated in detail.

Thanks very much for your suggestion. We evaluated the HER performance on D-$Ni(OH)_2$/Ni@CF and $Ni(OH)_2$/Ni@CF in 1 M KOH electrolyte without nitrate **(Figure 1)**. D-$Ni(OH)_2$/Ni@CF required an overpotential of only -0.19 V to reach a current density of 10 mA cm^{-2}, significantly lower than the overpotential needed for $Ni(OH)_2$/Ni@CF (-0.39 V). Furthermore, D-$Ni(OH)_2$/Ni@CF achieved a current density of 31.51 mA cm^{-2}, markedly surpassing $Ni(OH)_2$/Ni@CF of 12.22 mA cm^{-2} at -0.4 V vs. RHE. Despite the enhanced HER performance, D-$Ni(OH)_2$/Ni@CF also demonstrated superior NH_3 selectivity, further confirming the OH cycling mechanism on D-$Ni(OH)_2$/Ni@CF. Thus, we added the discussion in line 245 as follows: *"Additionally, D-$Ni(OH)_2$/Ni also showed better catalytic activity in the electrolyte without nitrate, implying its capability to reduce overpotential and promote proton transfer by optimizing hydroxyl adsorption and water dissociation (Fig. S30)"*

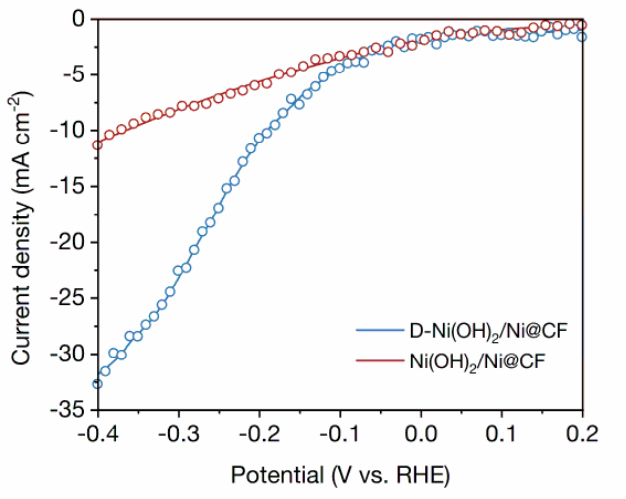

Figure 1 (Fig. S30 in SI). Polarization curves measured by linear sweep voltammetry (LSV) from 0.2 to -0.4 V vs. RHE of D-Ni(OH)$_2$/Ni@CF and Ni(OH)$_2$/Ni@CF in the electrolyte without nitrate.

Thank you very much for these valuable suggestions to help us get insight into the mechanism. We have completely updated the manuscript. Sincerely thank you for improving the quality of this manuscript!

Reviewer #3 (Remarks to the Author):

In this manuscript, a potential-dependent phase change was observed with Ni(OH)$_2$ as the electrocatalyst during nitrate reduction reaction (NO_3RR), while an OH cycle mechanism was proposed regarding the formation of a local-hydroxyl-enrich nanoconfined reaction surface to promote hydrogenation process. By further constructing more surface vacancies via plasma treatment, excellent NO_3RR performance can be achieved on D-Ni(OH)$_2$/Ni@CF. Despite good NO_3RR performance and some new insights from the authors, this reviewer still has several critical comments.

The first is that how the OH from the catalyst participates in/promotes NO_3RR to NH_3 process, considering that there is much OH in the alkaline electrolyte already? The authors need to give detailed discussion.

Thanks very much for your valuable suggestion. We also believed that the OH- in electrolyte will also participate in NO_3RR. Even though, previous work has rarely considered OH cycle during NO_3RR, the objective of this work was to hope to identify the potential existence of OH cycle at dynamic catalyst interface and elucidate its role involving in NO_3RR and promoting the reaction kinetics. In fact, the OH cycle mechanism, which is revealed by the experiments and related characterization, can efficiently illustrates that the real catalyst interface undergoes continuous reconstruction, while also being metastable interface and involved in proton transfer during the interaction with surface water. Based on characterization, it is assumed that the region of action for the OH cycle might be closer to the catalyst surface, displaying strong interaction with surface water in the process of nitrate hydrogenation.

Thus, we provided more detailed discussion about the role of the OH from the catalyst in NO_3RR. We specific prepared isotopically labeled $Ni(OD)_2$/Ni@CF catalyst and tried to trace the evolution of OH/OD species during the reaction, which was characterized by in situ DEMS and in situ FTIR. First, the $Ni(OH)_2$/Ni@CF catalyst was labeled through electrocatalysis in an electrolyte containing H_2O and D_2O as solvents, respectively **(Figure 1a, Figure 2a)**. Subsequently, NO_3RR was conducted in an electrolyte with H_2O as the solvent after thorough washing. The gas generated during the reaction was measured using DEMS. In the initial step, due to the exchange between lattice OH in the catalyst and OD in the solution, $Ni(OD)_2$/Ni@CF catalyst containing OD species was formed. If the OD in the $Ni(OD)_2$/Ni@CF catalyst participated in reaction, NH_xD_{3-x} product was expected to be produced in the subsequent step. As anticipated, NH_xD_{3-x} signals (m/z=18, 19, 20) were observed, providing direct and solid experimental evidence to confirm the OH cycle on the $Ni(OH)_2$/Ni@CF surface **(Figure 1b-e)**. However, no NH_xD_{3-x} species were observed on the catalyst pretreated with H_2O solvent, excluding signal interference or error caused by possible contaminants **(Figure 2b-c)**.

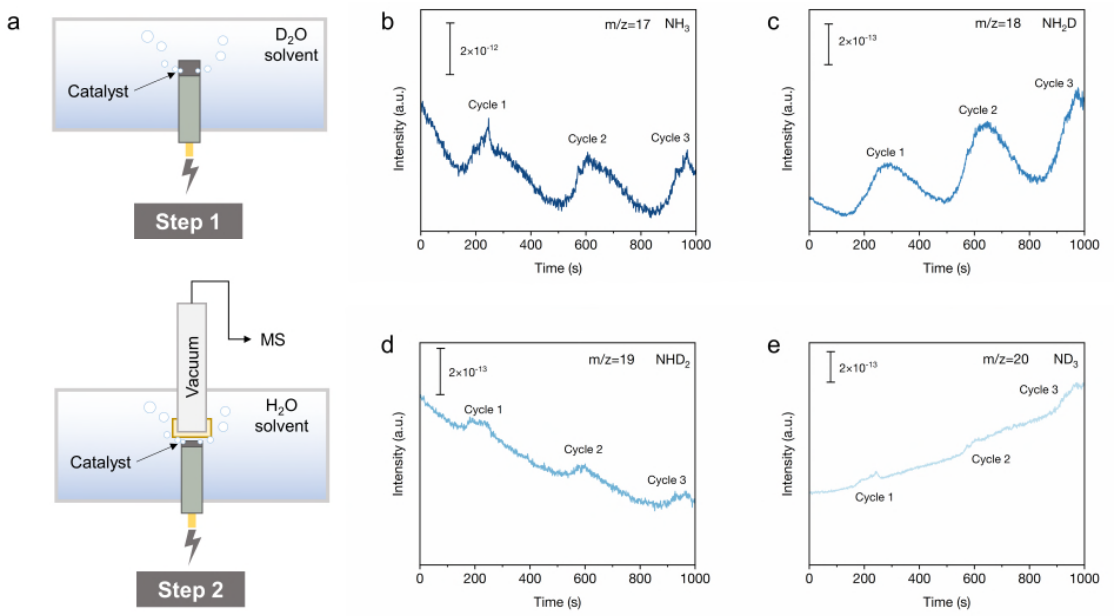

Figure 1 (Fig. S12 in SI). (a) Schematic diagram of the DEMS test with D_2O solvent pretreatment. Signals obtained by DEMS during NO_3RR. **(b)** m/z=17, **(c)** m/z=18. **(d)** m/z=19, **(e)** m/z=20.

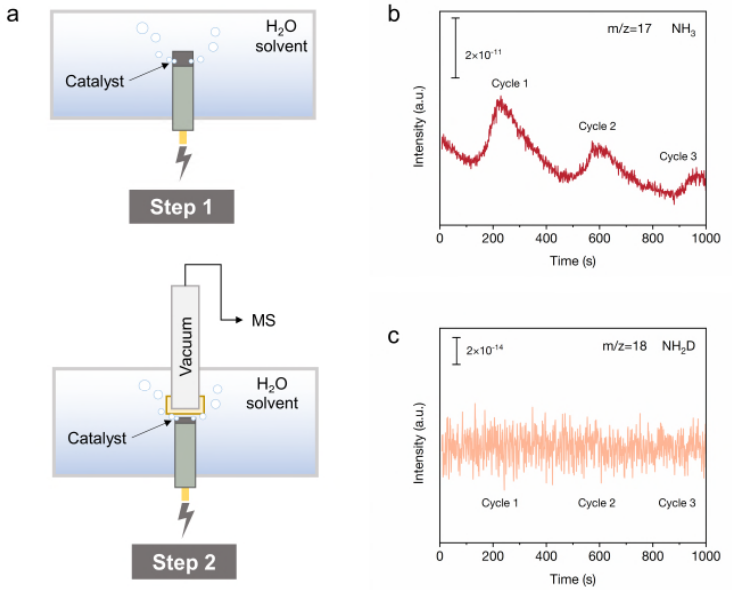

Figure 2 (Fig. S13 in SI). (a) Schematic diagram of the DEMS test with H_2O solvent pretreatment. Signals obtained by DEMS during NO_3RR. **(b)** m/z=17, **(c)** m/z=18.

Besides, serial isotope-labeling experiments were designed to elucidate the role of OH migration as well as the interplay between catalyst surface and electrolyte during NO3RR **(Figure 3)**. Initially, the $Ni(OD)_2$@CF catalyst prepared via D_2O was employed for NO_3RR with H_2O-based electrolyte. ATR-FTIR was utilized to characterize the electrolyte, and the peaks attributed to D_2O/DHO species was observed, indicating the exchange of lattice OD and solvent OH **(Figure 4a, Figure 5a)**. After

step I, we refreshed the electrolyte and continued NO_3RR, while almost no D_2O and NH_xD_{3-x} was detected in step II, confirming the depletion of D-containing hydroxyl on the previous catalyst surface **(Figure 4b, Figure 5b)**. Subsequently, the catalyst was again soaked in D_2O at open circuit potential (OCP) in step III, and the D/H ratio of the electrolyte increased to 0.17 **(Figure 4c, Figure 5c)**. This phenomenon demonstrated that the $Ni(OD)_2/Ni$ interface was metastable rather than static, where the metallic Ni readily regenerated into $Ni(OD)_2$ by spontaneously bonding to the hydroxyl group in the solvent. This process was repeated to ensure accuracy and confirm its regularity and reproducibility in step V and VI **(Figure 4d-e, Figure 5d-e)**.

Therefore, the $Ni(OD)_2/Ni$@CF interface has a strong interaction with the surface water **(Figure 6).** The de-hydroxylation effect contributed to the OH in the electrocatalyst involved in the formation of surface water, and the metastable active sites were prone to adsorb OH to form Ni-OH, thereby activated the surface H_2O and promote the surface H_2O equilibrium to dissociate. Thus, high activity protons transferred and participated in the hydrogenation of N-species on the electrocatalyst.

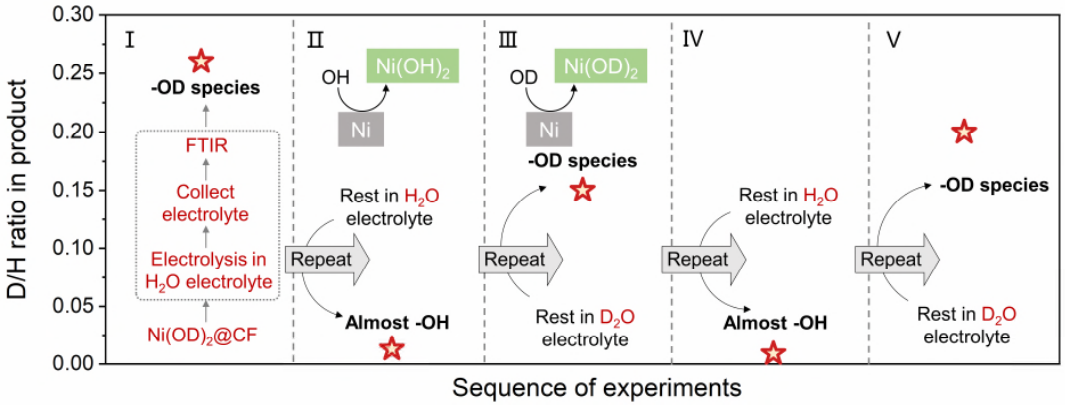

Figure 3 (Fig. S14 in SI). The semi-quantitative FTIR results of the D_2O and H_2O ratio in different operating conditions

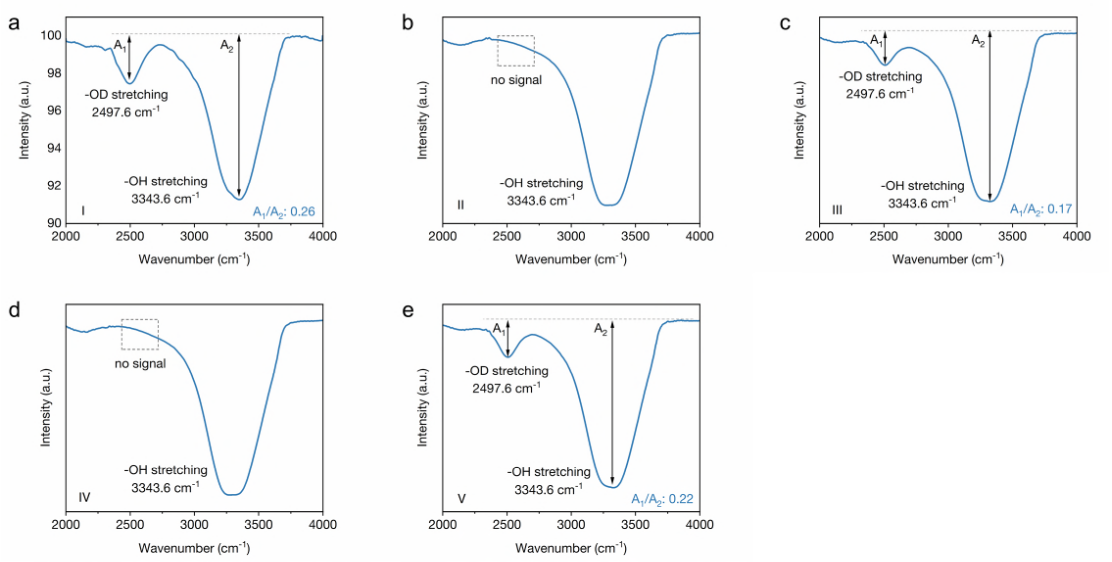

Figure 4 (Fig. S15 in SI). ATR-FTIR spectrum of the electrolyte corresponding to experiment I to V.

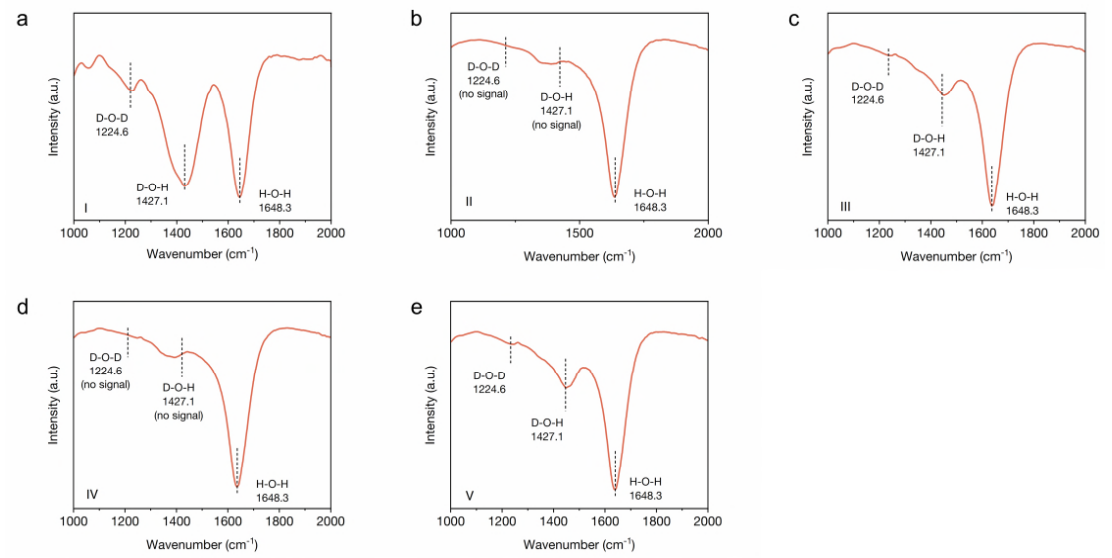

Figure 5. ATR-FTIR spectrum from 1000 to 2000 cm^{-1} of the electrolyte corresponding to experiment I to V.

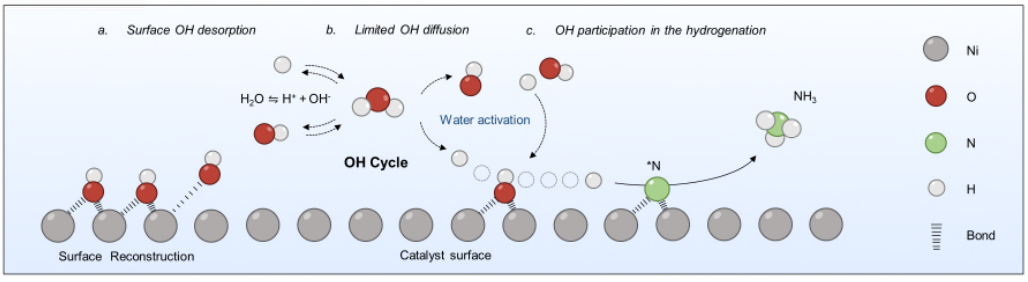

Figure 6 (Fig. 2f in manuscript). Schematic diagram during NO_3RR process including OH cycle mechanism.

We further supplemented the corresponding discussion in line 153 as follows: *"In-situ*

differential electrochemical mass spectrometry (DEMS) measurements were further carried out using H/D isotopic labeling to understand the OH evolution process. Firstly, the catalyst was labeled by operating in the electrolyte with H_2O and D_2O solvent, respectively. Then, NO_3RR was performed in the electrolyte with H_2O solvent after thoroughly washing, and the generated volatile products were measured using DEMS (Fig. S12-13) [28]*. As predicted, NH_xD_{3-x} signals (m/z=18, 19, and 20) assigned to NH_2D, NHD_2, and ND_3 was only detected on the catalyst pretreated in D_2O solvent, providing solid evidence to the interchange between lattice OH and electrolyte OD during the reaction (Fig. 2b-c)* [29]*.*

To further elucidate the role of OH migration as well as the interplay between catalyst surface and electrolyte during NO_3RR, serial isotopic labeling experiments were designed to trace the dynamic interface behavior using Attenuated total reflection Fourier transformed infrared (ATR-FTIR) (Fig. S14). (I) Initially, the $Ni(OD)_2$@CF catalyst prepared via D_2O was employed for NO3RR with H_2O-based electrolyte. The peak located at 2497.7 cm-1 and 3343.6 cm-1 was discerned, assigning to D_2O and H_2O species, respectively (Fig. S15). The semi-quantitative ratio of D_2O/H_2O (D/H) determined by FTIR was 0.26, consistent with the result of Raman spectra (Fig. S16-17). The appearance of D_2O species implied that the interfacial OH from catalyst participated in NO_3RR with water as a medium via the equilibrium of water dissociation.".

The second is that is it possible that the as-generated Ni/$Ni(OH)_2$ with suitable binding energies of reaction intermediates contributes to the good NO_3RR performance, rather than OH cycle?

Thank you very much for your suggestion. We further investigated the effects of the catalyst electronic structure modulation on NO_3RR performance via a series of experiments. A series of $Ni(OH)_2$/Ni catalysts with different ratios were prepared by adjusting the parameters during electrodeposition. To be specific, cyclic voltammetry electrodeposition for 6 cycles (0.1 mV/s) in the range of -1~0.5 V vs. RHE was performed, followed by 600 s potentiostatic electrodeposition at -1.1, -1.2, -1.3, -1.4, -1.5 V vs. Ag/AgCl for $Ni(OH)_2$@CF, $Ni(OH)_2/Ni_{7:3}$@CF, $Ni(OH)_2/Ni_{5:5}$@CF, $Ni(OH)_2/Ni_{3:7}$@CF and Ni@CF, respectively. XRD patterns demonstrated that the catalyst was composed of $Ni(OH)_2$/Ni heterostructures with different ratio **(Figure 1)**. The ratio of $Ni(OH)_2$ and Ni can be determined by the Ni^{2+} and Ni^0 peaks area in Ni 2p XPS spectra **(Figure 2)**.

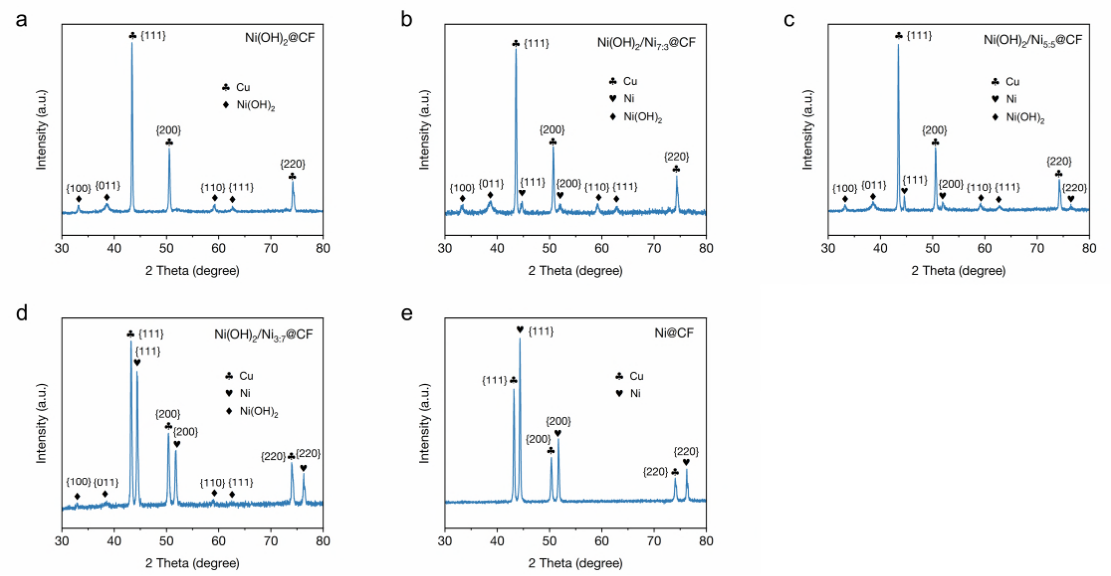

Figure 1 (Fig. S43 in SI). XRD patterns of $Ni(OH)_2$@CF, $Ni(OH)_2/Ni_{7:3}$@CF, $Ni(OH)_2/Ni_{5:5}$@CF, $Ni(OH)_2/Ni_{3:7}$@CF, and Ni@CF.

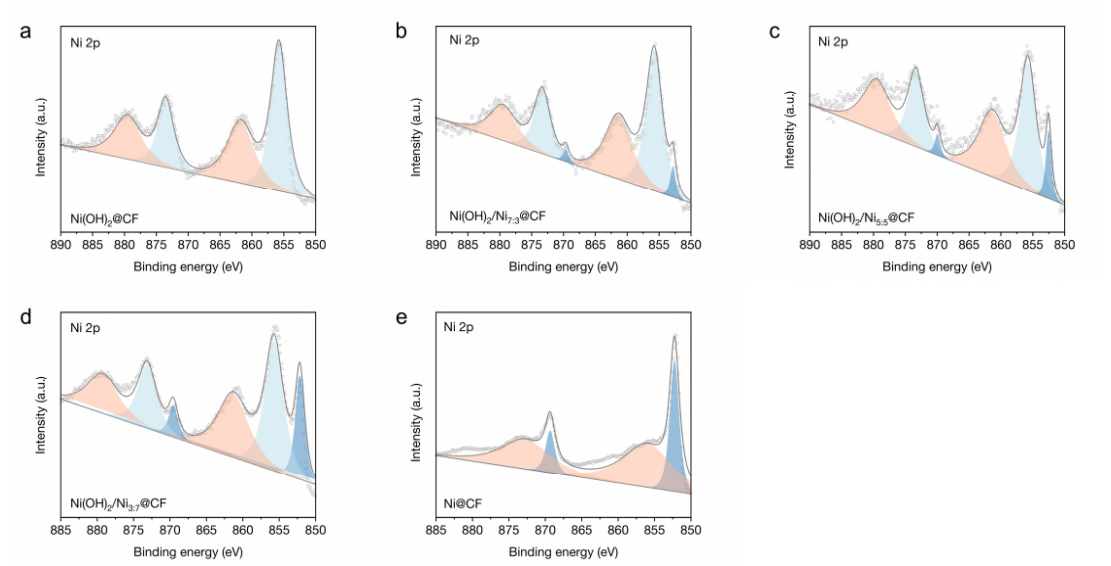

Figure 2 (Fig. S44 in SI). XPS Ni 2p spectra of $Ni(OH)_2$@CF, $Ni(OH)_2/Ni_{7:3}$@CF, $Ni(OH)_2/Ni_{5:5}$@CF, $Ni(OH)_2/Ni_{3:7}$@CF, and Ni@CF.

The above catalysts covered all ratios of $Ni(OH)_2$/Ni, which can fully reflect the influence of the mixed structure of $Ni(OH)_2$/Ni on the NH_3 synthesis performance. Thus, the electrochemical analysis was performed by using a typical three-electrode system, with the prepared catalyst as the working electrode, an Ag/AgCl electrode (filled with 3 M KCl) as the reference electrode, and a Pt foil as the counter electrode, respectively. The polarization curves of each electrocatalyst were measured **(Figure 3)**. By increasing the metallic Ni phase in $Ni(OH)_2$/Ni heterogeneous structure, the current density initially raised and then declined, demonstrating a volcano trend. This suggested that a

proper regulation of the $Ni(OH)_2/Ni$ structure indeed enhanced the electrocatalytic performance to a certain extent. However, employing such strategy reached a maximum current density of only -335.9 mA cm^{-2} on $Ni(OH)_2/Ni_{5:5}$@CF, significantly lower than -395.8 mA cm^{-2} achieved through activation of the OH cycle on D- $Ni(OH)_2/Ni$@CF **(Figure 4)**. Further, we also evaluated the FE (Faradaic efficiency) during NH_3 synthesis. It was hardly to increase the selectivity of NH_3 synthesis comparable to that of D-$Ni(OH)_2/Ni$@CF (FE=~100%) by only adjusting the $Ni(OH)_2/Ni$ structure (FE=50%-70%), which also implied the increase activity might be also originated from the defects and the enhanced OH cycle not only the effect of catalyst structure.

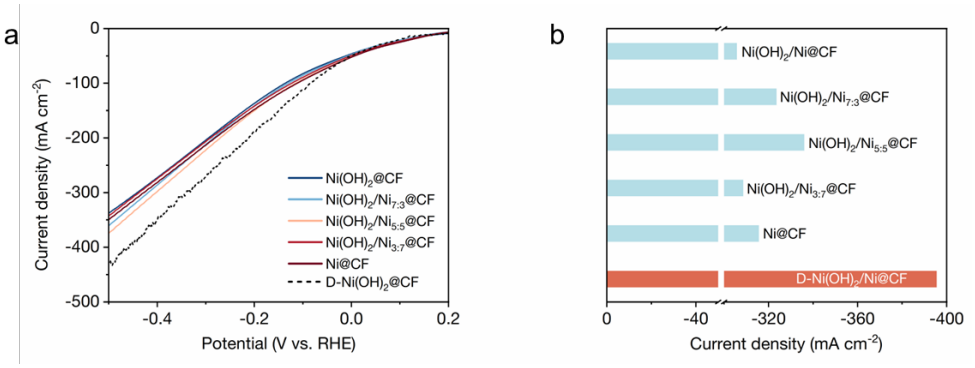

Figure 3 (Fig. S45 in SI). **(a)** Polarization curves from 0.2 to -0.5 V vs. RHE on $Ni(OH)_2$@CF, $Ni(OH)_2/Ni_{7:3}$@CF, $Ni(OH)_2/Ni_{5:5}$@CF, $Ni(OH)_2/Ni_{3:7}$@CF, Ni@CF, and D-$Ni(OH)_2$@CF catalysts. **(b)** Corresponding current density at -0.5 V vs. RHE.

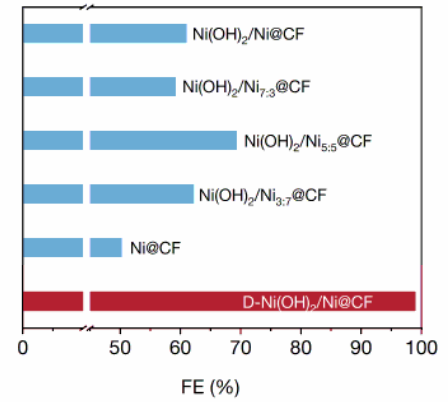

Figure 4 (Fig. S46 in SI). **(a)** FE of NH_3 synthesis at -0.6 V vs. RHE on $Ni(OH)_2$@CF, $Ni(OH)_2/Ni_{7:3}$@CF, $Ni(OH)_2/Ni_{5:5}$@CF, $Ni(OH)_2/Ni_{3:7}$@CF, Ni@CF, and D-$Ni(OH)_2$@CF catalysts.

Thus, we have supplemented the corresponding discussion in line 321 as follows: *"Furthermore, a range of $Ni(OH)_2/Ni$ catalysts with varying proportions were synthesized to distinguish the impacts of OH cycle and electronic structure modulation (Fig. S43-44). The current density of the $Ni(OH)_2/Ni$ heterogeneous structure demonstrated a volcano trend with the augmentation of the metallic Ni phase.*

The maximum current density of $Ni(OH)_2/Ni_{5:5}$@CF approached -335.9 mA cm^{-2}, while was still lower than that of D-$Ni(OH)_2$/Ni@CF (-395.8 mA cm^{-2}) (Fig. S45). Moveover, the FE of $Ni(OH)_2$/Ni heterogeneous structure (FE=50-70%) was notably inferior to that of D-$Ni(OH)_2$/Ni@CF (FE=100%), corroborating that the superior catalytic performance of D-$Ni(OH)_2$/Ni@CF, which might be also originated from the defects and the enhanced OH cycle not only the effect of catalyst structure (Fig. S46)"

This reviewer supposes that when hydroxyl vacancies are introduced in D-$Ni(OH)_2$/Ni@CF, more Ni species are generated during NO_3RR, and the as-generated Ni is responsible for water splitting to provide enough H for NO_3RR, leading to greatly enhanced NO_3RR performance. Overall, the mechanism understanding is not clear at this stage, which needs more exploration and discussion. Some additional suggestions are also listed as below:

1. In this contribution, Cu foam is used as the substrate. Is it possible that Cu atoms dissolve and deposit on or doped in the catalyst for enhanced NO_3RR performance, as Cu is generally regarded as a highly active electrocatalyst for NO_3RR.

Thank you very much for this question. When Cu foam was utilized as a substrate, the dissolved Cu atoms potentially infiltrated the Ni species, leading to a misinterpretation of catalytic activity origin. To confirm whether Cu interfered with the Ni catalyst, we stripped the surface of the catalyst and conducted a series of characterizations. ICP-OES results revealed the absence of Cu on the catalyst surface **(Table 1)**. Additionally, the imperceptible Cu signal in XPS spectra further demonstrated that Cu was not incorporated into the surface Ni species **(Figure 1)**.

Thus, we have supplemented the corresponding discussion in line 105 as follows: *"Besides, the prepared catalyst was stripped and characterized independently via X-ray photoelectron spectroscopy (XPS) and inductively coupled plasma optical emission spectrometer (ICP), which confirmed the absence of Cu on the catalyst surface and excluded the potential influence of Cu on enhanced reaction activity (Table. S1, Fig. S5)."*

Table 1 (Tabel. S1 in SI). ICP-OES results of the surface catalyst after electrocatalysis (ND: not detected).

Element	C_0 (mg/L)
Ni	6.641
Cu	ND
Co	ND

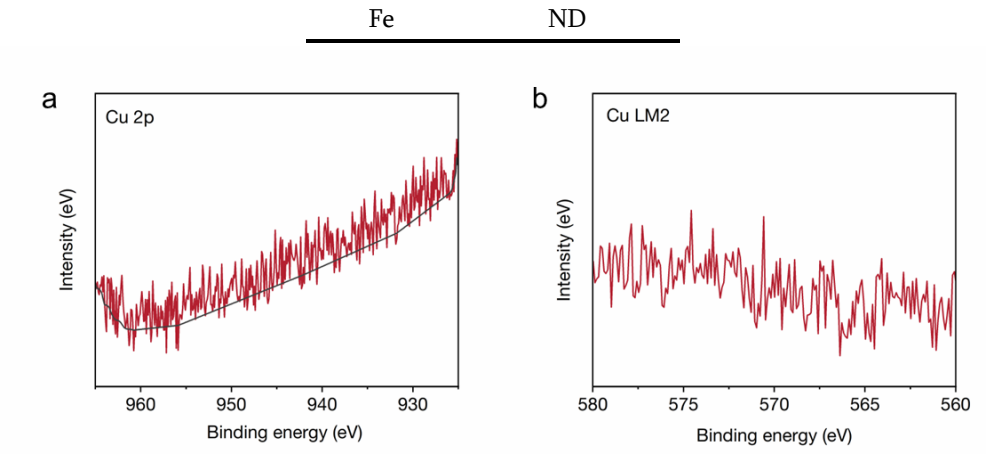

Figure 1 (Fig. S5 in SI). XPS spectra of the surface catalyst after electrocatalysis. **(a)** Cu 2p spectra. **(b)** Cu LM2 spectra.

2. The authors claim that structural reconstruction takes place at the top layers of the catalyst surface. However, as shown in fig. 2c, the newly formed Ni is in the inner area, which is coved by surface $Ni(OH)_2$.

Thanks very much for this question, and we are very sorry for the misleading. Given that we employed electrodeposition for the in-situ growth of the self-supporting Ni species onto the substrate, the surface catalyst necessitated ultrasonic stripping before TEM characterization. Consequently, it is not possible to distinguish between the inner and outer regions of the catalyst in TEM result.

Due to the surface sensitivity of Raman spectroscopy [1], the diminishment of Ni-OH signal conclusively indicated the process from Ni^{2+} to Ni^0 occurred on the catalyst surface **(Figure 1)**. Further, it has been proved that the surface reconstruction induced by electric potential typically initiated at the electrode-electrolyte interface, spanning several atomic layers, prior to the spreading into bulk phase [2]. Hence, we confirmed the reliability of our conclusion regarding the inner $Ni(OH)_2$ and outer Ni configuration of the catalyst.

Finally, to enhance the readability and mitigate reader's confusion, we replaced **Figure 1** with an alternative TEM image.

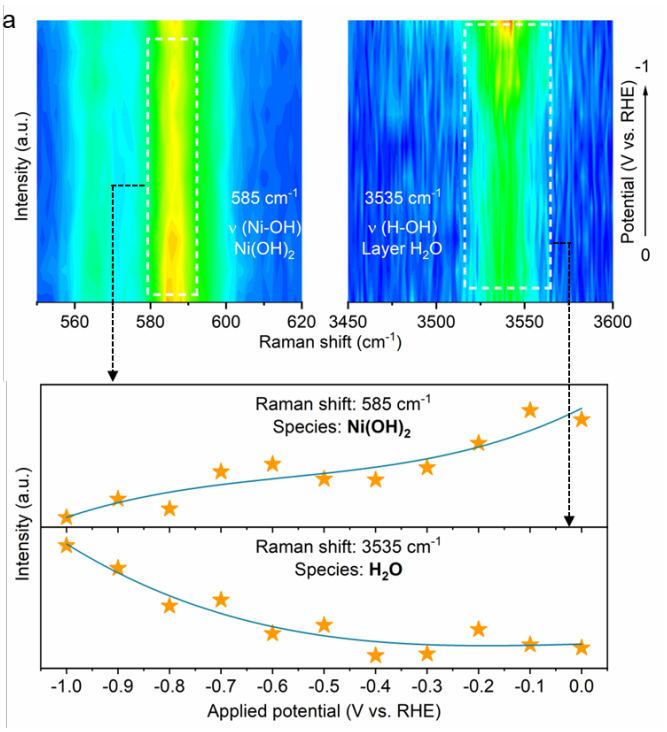

Figure 1 (Fig. 2a in manuscript). In situ electrochemical Raman spectra of $Ni(OH)_2$/Ni@CF from 0 to -1.0 V vs. RHE in the electrolyte with 0.1 M KNO_3 + 1 M KOH. Below: The intensity of the Raman signal at 585 cm^{-1} and 3535 cm^{-1} (scatter: real Raman signal; line: polynomial fitting curve).

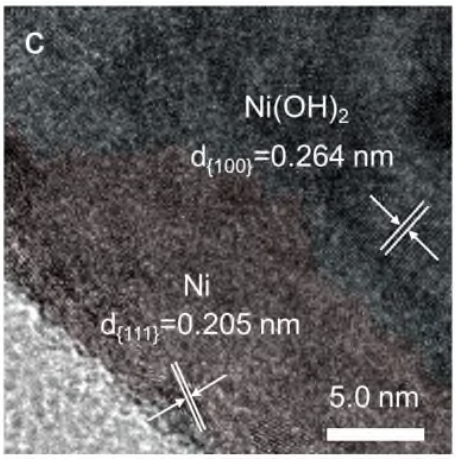

Figure 2 (Fig. 1c in manuscript). HR-TEM images of $Ni(OH)_2$/Ni@CF (scale bar: 5 nm).

[1] X. Han et al. Surface-enhanced Raman spectroscopy. *Nat. Rev.* **1**, 87 (2021).

[2] T. Li et al. Atomic-scale insights into surface species of electrocatalysts in three dimensions. *Nat. Catal.* **1**, 300-305 (2018).

3. Please label the XRD peak at near 35 degrees in fig. S4.

We highly appreciate the suggestion to improve this paper. We meticulously examined the XRD results with standard patterns, which indicated that the peaks near 35° could not be attributed to Cu, Ni, or $Ni(OH)_2$.

Upon careful comparison, the peaks at ~35° (37.2°) were attributed to the {110} crystal planes of NiO. We speculated that the prolonged storage of the sample before XRD characterization led to a slight oxidation of the surface Ni phase. Further, we conducted XRD tests on the catalyst preserved in vacuum and exposed to air. The results demonstrated that the sample preserved in vacuum eliminated the formation of NiO **(Figure 1-2)**.

Consequently, we have replaced Fig. S5 in the article to uphold the rigor of our findings. Thanks for your valuable suggestion.

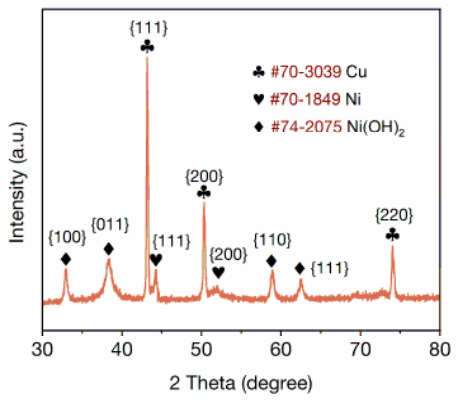

Figure 1 (Fig. S6 in SI). XRD pattern of $Ni(OH)_2$/Ni@CF after electrocatalysis (preserved in vacuum).

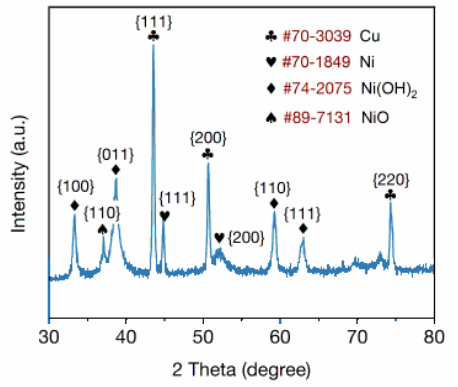

Figure 2. XRD pattern of $Ni(OH)_2$/Ni@CF after electrocatalysis (exposed to air).

4. "This phenomenon demonstrated that the $Ni(OH)_2$/Ni interface was not static, where the metallic Ni readily regenerated into $Ni(OH)_2$ by spontaneously bonding to the hydroxyl group in solvent." Here, should be $Ni(OD)_2$/Ni, not $Ni(OH)_2$/Ni.

Thanks very much for your correction. We have corrected the error and conducted a comprehensive review of the manuscript to prevent such mistakes.

5. As displayed in fig. 3d, $Ni(OH)_2/Ni$ surface has a better OH capture ability than Ni. However, the DFT results in fig. S12 only show the free energy diagram of NO_3RR process on Ni and $Ni(OH)_2$, while $Ni(OH)_2/Ni$ is the real catalyst for NO_3RR.

Thanks for your suggestion. We also realized the limitations of the modeling method used in the NO_3RR free energy calculation, thus updated the DFT calculation for $Ni(OH)_2/Ni$ **(Figure 1-3)**.

Further, we corrected the manuscript at line 188 as follows: *"Consistently, the energy barrier of the potential-determined step (PDS) on $Ni(OH)_2/Ni$ (0.48 eV) was lower than that of $Ni(OH)_2$ (1.40 eV) (Fig. S18-20, Table S3), and the crystal orbital Hamilton population (COHP) proved the better adsorption capacity for NO_3^- on $Ni(OH)_2/Ni$ (Fig. S21), revealing the genuine active site originated from $Ni(OH)_2/Ni$ surface."*

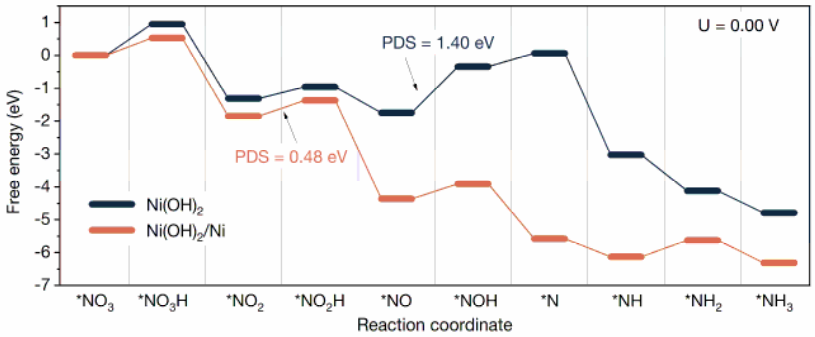

Figure 1 (Fig. S18 in SI). Free energy diagram of the NO_3RR process on $Ni(OH)_2$ and $Ni(OH)_2/Ni$.

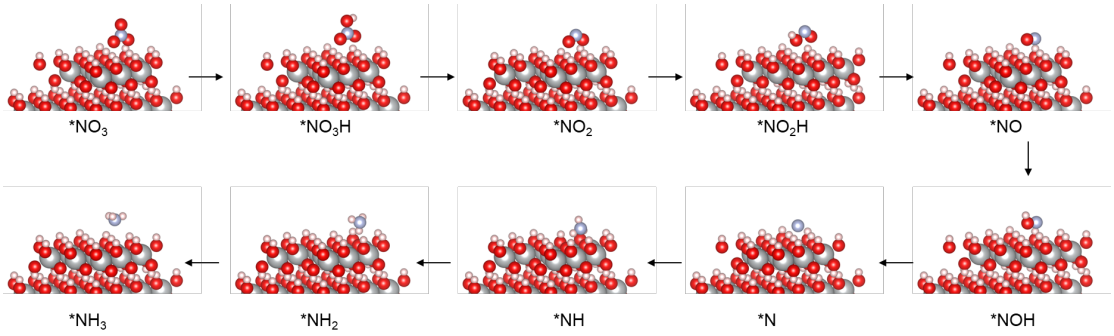

Figure 2 (Fig. S19 in SI). Models after structural relaxation on $Ni(OH)_2$ during nitrate reduction reaction process.

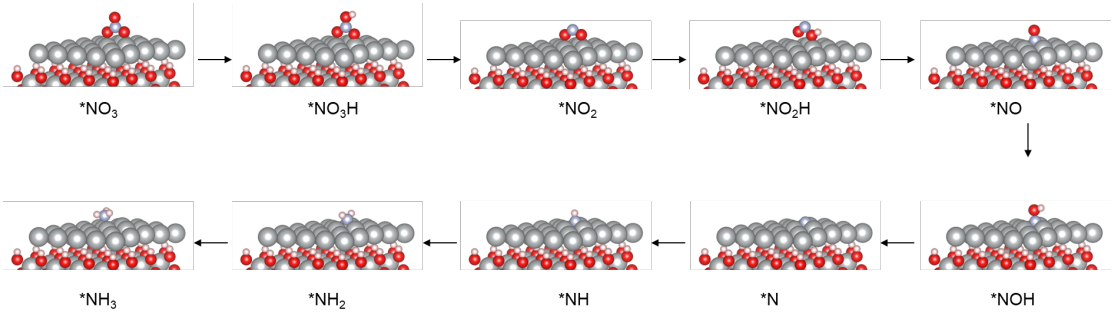

Figure 3 (Fig. S20 in SI). Models after structural relaxation on $Ni(OH)_2/Ni$ during nitrate reduction reaction process.

6. The authors demonstrate that the OH or OD from the catalyst participates in NO_3RR process. Can the authors explain how OH or OD reacts with NO_3^-, as it is generally suggested that the as-generated NH_3 capture the H from the decomposition of H_2O.

Thanks for your suggestion. The mechanism diagram for the process was shown in **Figure 1.** The dynamic process of surface OH desorption → limited OH diffusion → OH participation in the hydrogenation constituted the surface OH cycle. Due to the equilibrium of water dissociation, a dynamic exchange occurred between H_2O and OH (OD). We performed isotopic labeling on the $Ni(OD)_2/Ni$@CF catalyst followed by electrochemical measurements to track the behavior of OH species. The electrolyte after NO_3RR was measured via ATR-FTIR, and the peak at 2497 cm^{-1} indicated the generation of D_2O/HDO **(Figure 2-4)**. The metastable $Ni(OH)_2/Ni$ interface with strong OH adsorption ability activated the interfacial water dissociation, thus accelerated the proton transportation [1].

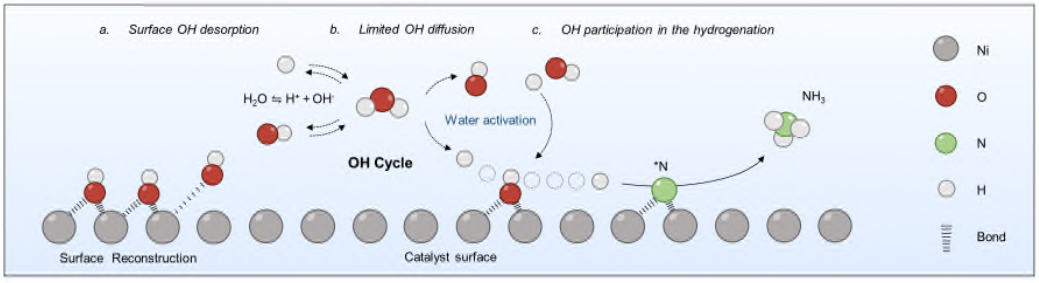

Figure 1 (Fig. 2f in manuscript). Schematic diagram during NO_3RR process including OH cycle mechanism.

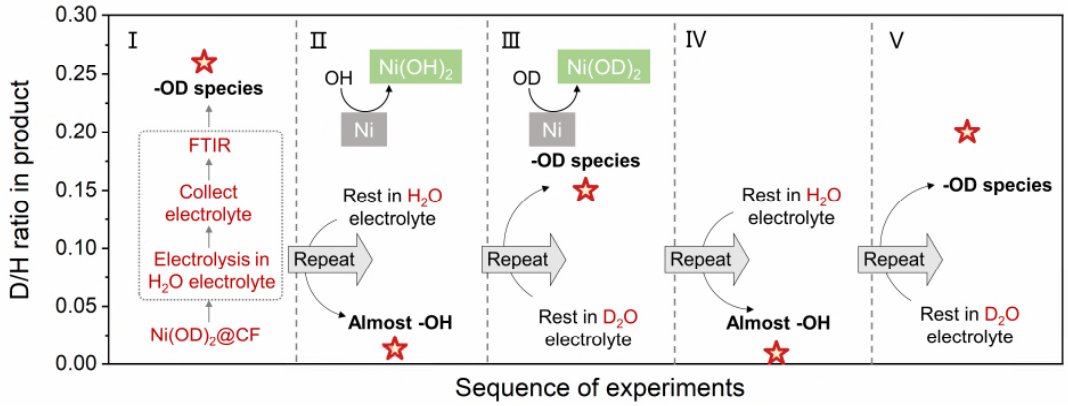

Figure 2 (Fig. S14 in SI). The semi-quantitative FTIR results of the D_2O and H_2O ratio in different operating conditions

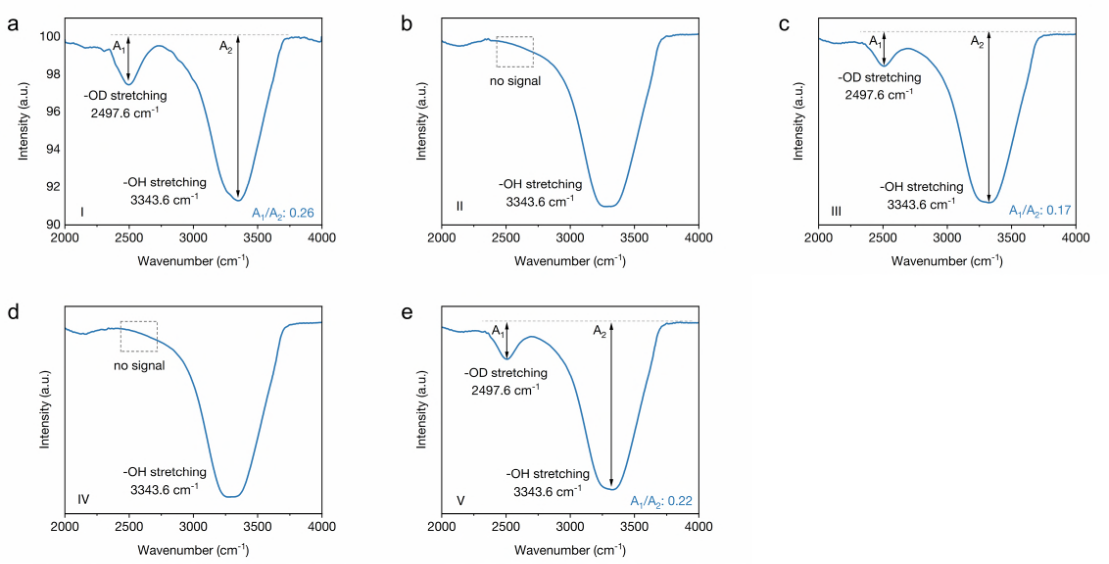

Figure 3 (Fig. S15 in SI). ATR-FTIR spectrum of the electrolyte corresponding to experiment I to V.

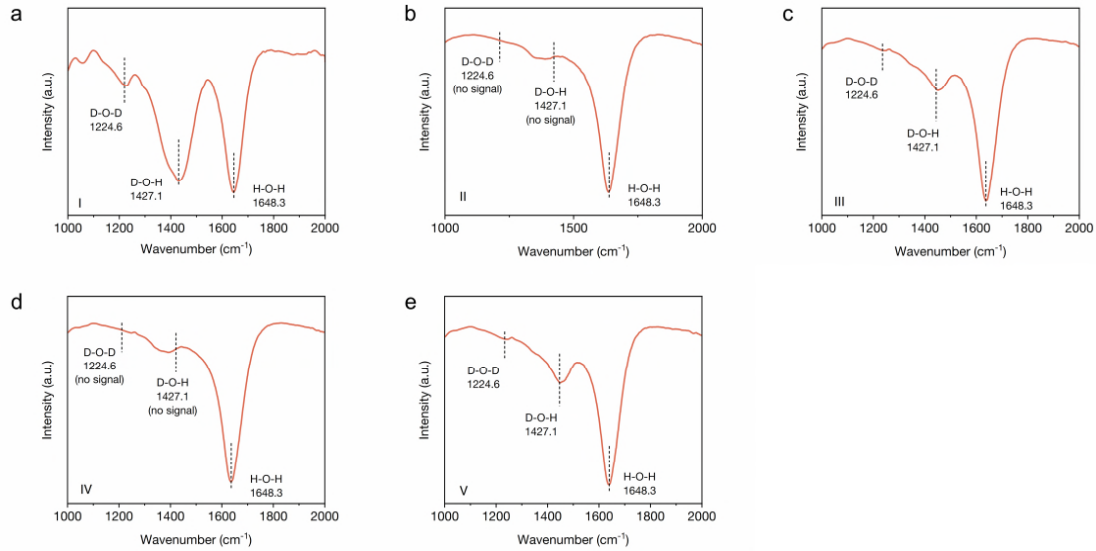

Figure 4. ATR-FTIR spectrum from 1000 to 2000 cm^{-1} of the electrolyte corresponding to experiment I to V.

Finally, we supplemented the corresponding discussion in line 153 as follows: *". In-situ differential electrochemical mass spectrometry (DEMS) measurements were further carried out using H/D isotopic labeling to understand the OH evolution process. Firstly, the catalyst was labeled by operating in the electrolyte with H_2O and D_2O solvent, respectively. Then, NO_3RR was performed in the electrolyte with H_2O solvent after thoroughly washing, and the generated volatile products were measured using DEMS (Fig. S12-13)* [28]*. As predicted, NH_xD_{3-x} signals (m/z=18, 19, and 20) assigned to NH_2D, NHD_2, and ND_3 was only detected on the catalyst pretreated in D_2O solvent, providing solid evidence to the interchange between lattice OH and electrolyte OD during the reaction (Fig. 2b-c)* [29]*.*

To further elucidate the role of OH migration and key intermediates during NH_3 synthesis, serial isotopic labeling experiments were designed to trace the dynamic interface behavior using Attenuated total reflection Fourier transformed infrared (ATR-FTIR) (Fig. S14). (I) Initially, the $Ni(OD)_2$@CF catalyst prepared via D_2O was employed for NO_3RR with H_2O-based electrolyte. The peak located at 2497.7 cm^{-1} and 3343.6 cm^{-1} was discerned, assigning to D_2O and H_2O species, respectively (Fig. S15). The semi-quantitative ratio of D_2O/H_2O (D/H) determined by FTIR was 0.26, which was also confirmed by Raman spectra (Fig. S16-17). The appearance of D_2O species implied that the interfacial OH from catalyst participated in NO_3RR with water as a medium via the equilibrium of water dissociation."

[1] X. Chen, J. Chen, H. Chen, Q. Zhang, J. Li, J. Cui, Y. Sun, D. Wang, J. Ye and L. Liu. *Nat. Commun.* 2023, **14**, 751.

7. Where is fig. 3e as mentioned by the authors?

Thanks very much for your question. We regretfully included an incorrect figure number in the manuscript, leading to unnecessary ambiguity. We have now rectified this error by updating all figure numbers to accurately correspond with the content presented in this manuscript.

8. Is it possible that the enhanced current density of D-Ni(OH)/Ni@CF from the LSV curve is only caused by the larger ECSA (fig. S20)?

Thanks very much for this question. To investigate whether ECSA was the origin of the catalytic activity enhancement, ECSA measurements were conducted immediately after the catalyst

preparation. The comparable ECSA values of D-Ni(OH)$_2$/Ni@CF and Ni(OH)$_2$/Ni@CF indicated that the defects caused by plasma did not greatly change the intrinsic activity **(Figure 1)**. The current density on D-Ni(OH)$_2$/Ni@CF was normalized to that of Ni(OH)$_2$/Ni@CF by ECSA:

$$j_{\text{ECSA normalized D-Ni(OH)2/Ni@CF}} = j_{\text{D-Ni(OH)2/Ni@CF}} * \text{ECSA}_{\text{Ni(OH)2/Ni@CF}} / \text{ECSA}_{\text{D-Ni(OH)2/Ni@CF}} \quad (1)$$

The catalytic activity remained superior, excluding the effect from the surface roughness modification by NTP **(Figure 2):**

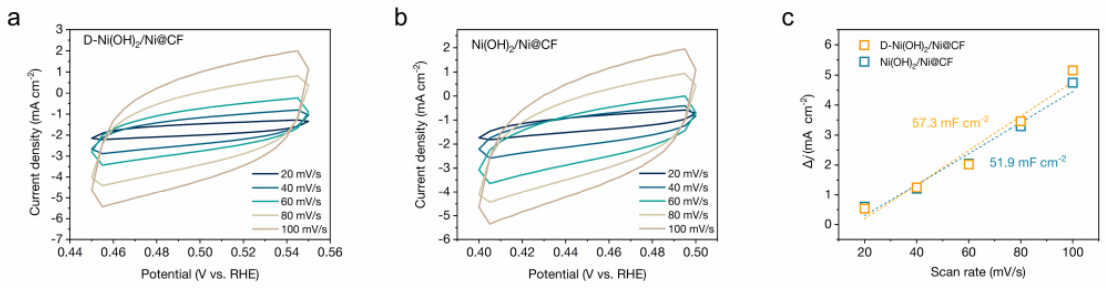

Figure 1 (Fig. S28-29 in SI). CV curves immediately after catalyst preparation in the non-faradaic area with different scan rates (20 mV/s, 40 mV/s, 60 mV/s, 80 mV/s, and 100 mV/s) of **(a)** D-Ni(OH)$_2$/Ni@CF and **(b)** Ni(OH)$_2$/Ni@CF. **(c)** The double layer capacitance (Cdl) of Ni(OH)$_2$/Ni@CF and D-Ni(OH)$_2$/Ni@CF immediately after catalyst preparation calculated by CV curves.

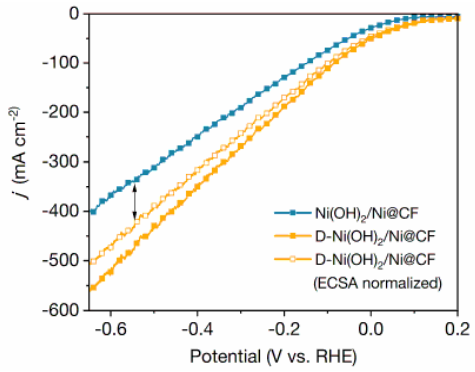

Figure 2 (Fig. 3g in manuscript). Polarization curves measured by linear sweep voltammetry (LSV) from 0.2 V vs. RHE to -0.65 V vs. RHE of Ni(OH)$_2$/Ni@CF, D-Ni(OH)$_2$/Ni@CF, and ECSA normalized D-Ni(OH)$_2$/Ni@CF ($j_{\text{ECSA normalized D-Ni(OH)2/Ni@CF}} = j_{\text{D-Ni(OH)2/Ni@CF}} * \text{ECSA}_{\text{Ni(OH)2/Ni@CF}} / \text{ECSA}_{\text{D-Ni(OH)2/Ni@CF}}$).

However, after series of electrochemical measurements, we performed ECSA measurement again and D-Ni(OH)/Ni@CF exhibited a larger ECSA than Ni(OH)/Ni@CF **(Figure 3)**. This phenomenon was attributed to the heightened exposure of metallic Ni sites facilitated by rapid OH cycle on the surface, a fact substantiated by in situ Raman spectroscopy **(Figure 4)**. Thus, the

enhanced current density on D-Ni(OH)2/Ni@CF was arisen from the fast OH cycle instead of the increasing surface area introduced by surface defects.

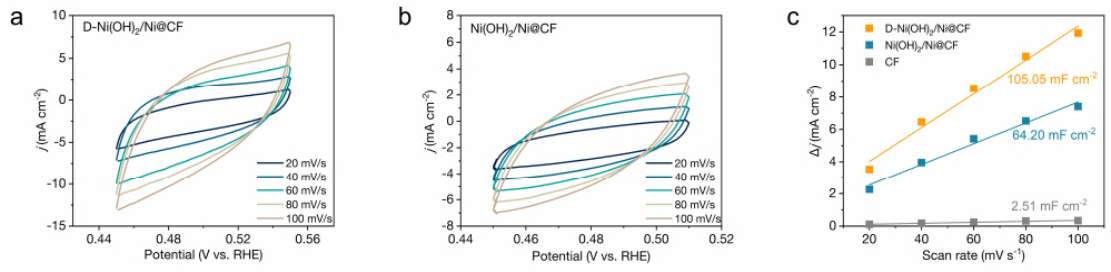

Figure 3 (Fig. S33-34 in SI). CV curves (after electrocatalysis) in the non-faradaic area with different scan rates (20 mV/s, 40 mV/s, 60 mV/s, 80 mV/s, and 100 mV/s) of **(a)** D-Ni(OH)2/Ni@CF and **(b)** Ni(OH)2/Ni@CF. **(c)** The double layer capacitance (Cdl) of Ni(OH)2/Ni@CF and D-Ni(OH)2/Ni@CF after electrocatalysis calculated by CV curves.

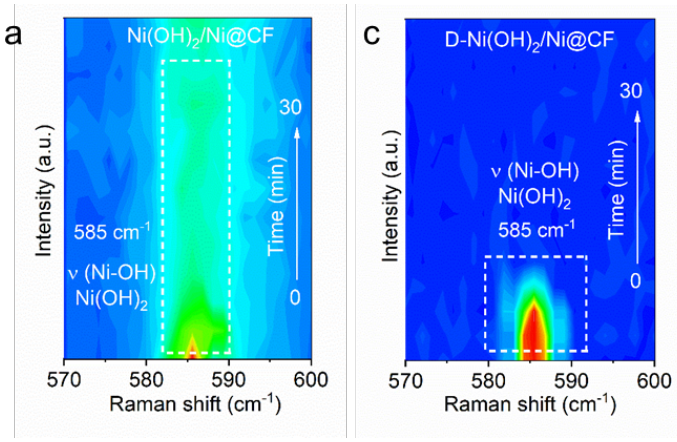

Figure 4 (Fig. 4a, 5c in manuscript). In situ electrochemical Raman spectra at -0.8 V vs. RHE of **(a)** Ni(OH)2/Ni@CF and **(c)** D-Ni(OH)2/Ni@CF with a time scale of 0~30 min.

Thus, We also supplemented the corresponding discussion in line 236 as follows: *"We initially evaluated the ESCA of the freshly prepared catalyst for comparison, revealing the comparable C_{dl} values for D-Ni(OH)2/Ni@CF (57.3 mF cm-2) and Ni(OH)2/Ni@CF (51.9 mF cm-2) (Fig. S28-29). Polarization curves exhibited a substantially lower overpotential and larger current density of D-Ni(OH)2/Ni@CF (-562.6 mA cm-2) compared to CF (157.63 mA cm-2) and Ni(OH)2/Ni (400.45 mA cm-2), indicating accelerated kinetics of NO3RR electrochemical reaction on activated interface (Fig. 3g). After normalizing the current density on D-Ni(OH)2/Ni@CF to that of Ni(OH)2/Ni@CF by ECSA, the catalytic activity remained superior (503.96 mA cm-2), excluding the effect from the surface roughness modification by NTP. Through long-term electrosynthesis of NH3, the ECSA on D-Ni(OH)2/Ni@CF*

(105.05 mF cm^{-2}) increased more significantly than that of Ni(OH)$_2$/Ni@CF (64.20 mF cm^{-2}), reflected the faster surface evolution on the activated dynamic interface with more active sites (Fig. S33-34)"

9. Pls avoid such simple mistakes like "Upon the addition of 1 M KNO$_3$", "fig. 5i", etc.

Thanks very much for your suggestion. We have thoroughly reviewed the manuscript, meticulously matched each figure number, and addressed minor errors. Thank you very much for your kind reminding for improving the quality of this manuscript.

10. Fig. 6g-h demonstrate the importance of accelerated H$_2$O dissociation kinetic to provide enough H for NO$_3$RR. So does it mean that the H in NH$_3$ mainly comes from the dissociation of water, rather than the OH from the catalyst.

Thanks for your suggestion. First, we also agreed that that H in NH$_3$ comes from the dynamic dissociation H of surface water as medium, rather than directly transfer from the OH of the electrocatalyst to adsorbed N-containing species. And the OH source could be both from the electrocatalyst and electrolyte. Actually, we have provided a detailed explanation of the evolution of OH during NO$_3$RR in our response to comment 6. The presence of -OD and NH$_x$D$_{3-x}$ species in the electrolyte suggested the potential involvement of -OD during NO$_3$RR **(Figure 1, Figure 2)**. However, their abundance appeared limited, as evidenced by the semi-quantitative -OH/-OD ratio (0.26, 0.17, 0.22) and the ration of m/z=18 to m/z=17 (~1/10). While not predominant, this process indeed represented a viable pathway that can facilitate reactions and significantly contribute to ongoing research aimed at elucidating the mechanism of NO$_3$RR.

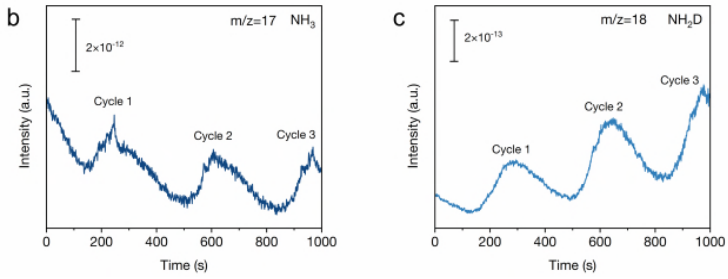

Figure 1 (Fig. S12 in SI). Signals obtained by DEMS during NO$_3$RR. **(b)** m/z=17, **(c)** m/z=18.

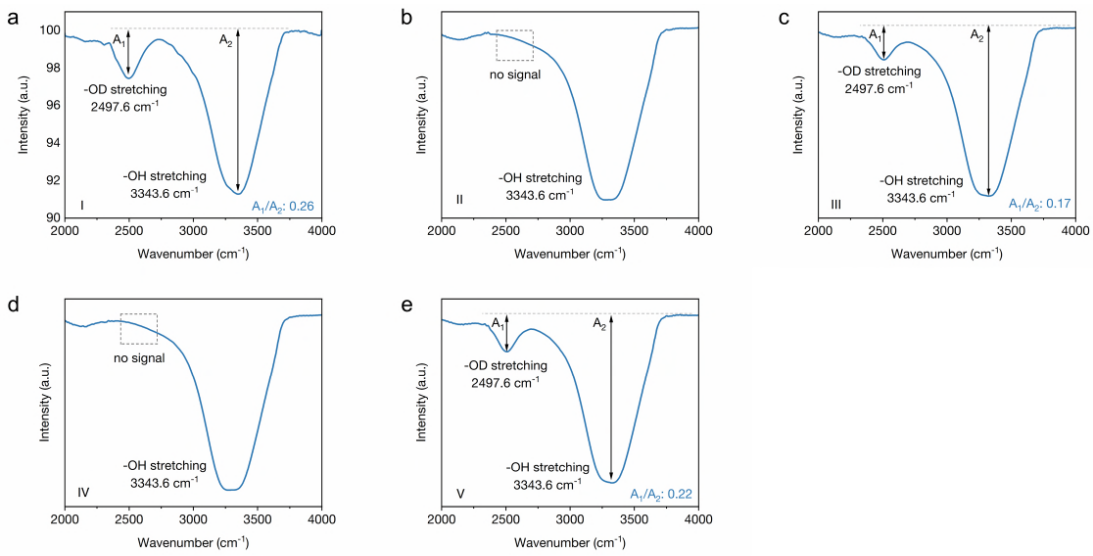

Figure 2 (Fig. S15 in SI). ATR-FTIR spectrum of the electrolyte corresponding to experiment I to V.

Furthermore, it is interesting that D-Ni(OH)2/Ni@CF exhibited not only a faster NH3 production rate compared to Ni(OH)2/Ni@CF, but also reached ~100% FE **(Figure 3)**. Typically, the defect facilitated the exposed Ni and strengthen the adsorption of OH-, with the formation of local high alkaline region, thereby inhibiting the competitive HER, indicating that a mere increase in H2O dissociation rate cannot solely explain the origin of enhanced catalytic activity compared to the rapid OH cycle.

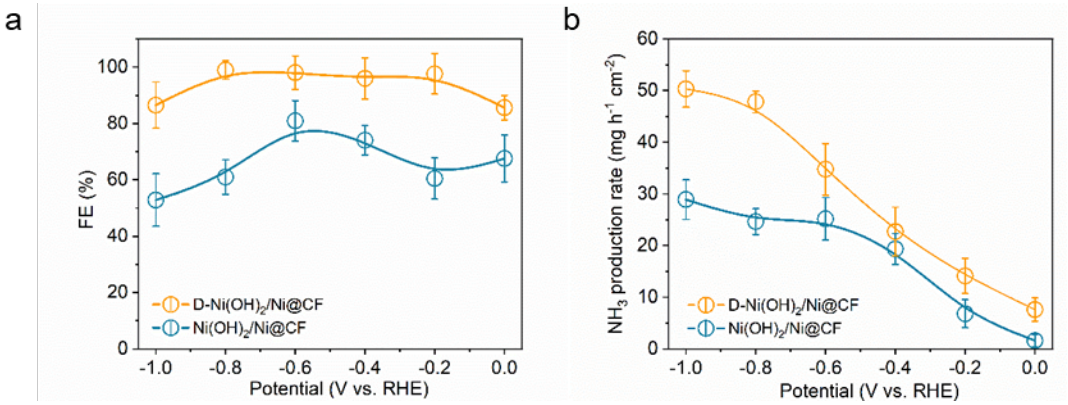

Figure 3 (Fig. 5a-b in manuscript). **(a)** FE and **(b)** NH3 production rate on Ni(OH)2/Ni@CF and D-Ni(OH)2/Ni@CF at the potential range from 0.0 to -1.0 V vs. RHE.

Thank you very much for these valuable suggestions to help us get insight into the mechanism. We have completely updated the manuscript. Sincerely thank you for improving the quality of this manuscript!

REVIEWER COMMENTS

Reviewer #1 (Remarks to the Author):

In the revised manuscript, the authors have some concerns raised before. However, there are still some problems that need to be addressed. I am still confused about the generation of OH radicals under reduction conditions. In the cited reference “fast oxygen exchange between HCO_3^- and H_2O provides oxygen sources for the formation of OH• radicals”, but in this work, what causes the generation of OH• radicals? The authors should explain it more clearly. Besides, Fe, Co, and Ni could spontaneously react with nitrate in the solution and then turn into their hydroxide form (Nat. Catal. 2023, 6, 402-414). At this time, nitrate is reduced to nitrite. It is recommended the authors reconsidered the generation $Ni(OH)_2$ and OH• radicals in NO_3 RR.

1. In Fig. 1e-f, the author stressed that the strength of the Ni-O bond in $Ni(OH)_2$/Ni@CF is decayed than $Ni(OH)_2$@CF using the Wavelet transformation analysis. However, in the Fourier transformation analysis or the R space results shown in the inset of Fig. 1e, the intensity of the Ni-O bond about 1.8 Å in $Ni(OH)_2$/Ni@CF is stronger than that on $Ni(OH)_2$@CF. The Wavelet transformation and the Fourier transformation are only two different treatment methods on the same data. The conclusions should remain consistent. Besides, the color scale bars are missing in Fig. 1f and g.
2. In Fig. 3h and I, the selected potential range is from +0.7 V to -0.1 V. What is the purpose of performing the EIS test from +0.7 V? Especially, the bode plots for D-$Ni(OH)_2$/Ni@CF is confusing. There is no obvious pattern. For example, is the phase angle for low low-frequency part is obvious than the high-frequency part for D-$Ni(OH)_2$/Ni@CF between +0.7 V to +0.5V?
3. In Figures 4b and d, the peaks at 2915 cm^{-1} and 2849 cm^{-1} were assigned to H-N-H. As the IR vibration at this range is usually related to vibration in C-H (J. Phys. Chem. 1996, 100, 25, 10664-10672), the authors should provide references or more experiments for support their conclusion.
4. In Figure S35, the Raman data seems strange. The peak looks like a broken line. The sampling step should be adjusted.
5. The TEA of the generated NH_3 production process seems meaningless. Why the electrochemical system cost was calculated to be 968 $/kW? Based on what? It would be better if the authors provided a detailed calculation process. Considering the stability duration of D-$Ni(OH)_2$/Ni@CF is only 24 h, the calculation method seems suspectable.

Reviewer #3 (Remarks to the Author):

In the revised manuscript, the authors have properly addressed all the questions raised by the reviewers, and the revised paper is ready for acceptance now.

Dear Editor and Reviewer:

Sincerely, thank you very much for your time and effort to carefully review and examine our manuscript. We greatly appreciate for this opportunity to revise the paper based on very insightful and helpful comments, which is important to ensure the quality and accuracy of our work. In response to the editor's concerns and the reviewer's suggestions, we have carefully made the revisions point by point with supplementary characterization and calculation, which have been marked in red in the revised manuscript and supplementary material. The corresponding revisions are specified and discussed in detail as follows:

Reviewer #1

In the revised manuscript, the authors have some concerns raised before. However, there are still some problems that need to be addressed. I am still confused about the generation of OH radicals under reduction conditions. In the cited reference “fast oxygen exchange between HCO_3^- and H_2O provides oxygen sources for the formation of OH• radicals”, but in this work, what causes the generation of OH• radicals? The authors should explain it more clearly. Besides, Fe, Co, and Ni could spontaneously react with nitrate in the solution and then turn into their hydroxide form (Nat. Catal. 2023, 6, 402-414). At this time, nitrate is reduced to nitrite. It is recommended the authors reconsidered the generation $Ni(OH)_2$ and OH• radicals in NO_3 RR.

Thank you very much for this comment, which also puzzled us why highly oxidizing species appeared at reduction condition. Previously, we speculated OH radicals may exist during reaction, according to the occurrence of DMPO-OH signal based on repeated quasi in-situ EPR tests. After extensive literature review, we realized the above statement may be not entirely rigorous, as the DMPO-OH species may be generated via different routes. Typically, at oxidation condition for application (such as water treatment), the presence of the DMPO-OH signal may indicate that the presence of OH radical based the reaction between OH radicals with the DMPO trapping agent. However, there is also alternative pathway for the formation of DMPO-OH signal, such as direct nucleophilic addition of DMPO by H_2O [1], or the cracking of DMPO-R [2], etc.

To identify the origin of the DMPO-OH signal in our system, we conducted a series of experiments. The DMPO-OH signal was detected in the reduction-potential-system both in the

presence and absence of NO_3^- (1 M KOH and 1 M KOH + 0.1 M KNO_3) and surface defects ($Ni(OH)_2$/Ni@CF and D-$Ni(OH)_2$/Ni@CF). However, no DMPO-OH signal was observed with $Ni(OH)_2$ surface under open circuit potential (OCP) conditions **(Figure 0-1 a-b)**. Furthermore, no DMPO-OH signal was observed on Ni@CF in KOH **(Figure 0-1 c)**. Thus, we speculated that the reconstruction process of $Ni(OH)_2 \rightarrow Ni(OH)_2$/Ni induced by negative potential may be crucial to the formation of DMPO-OH.

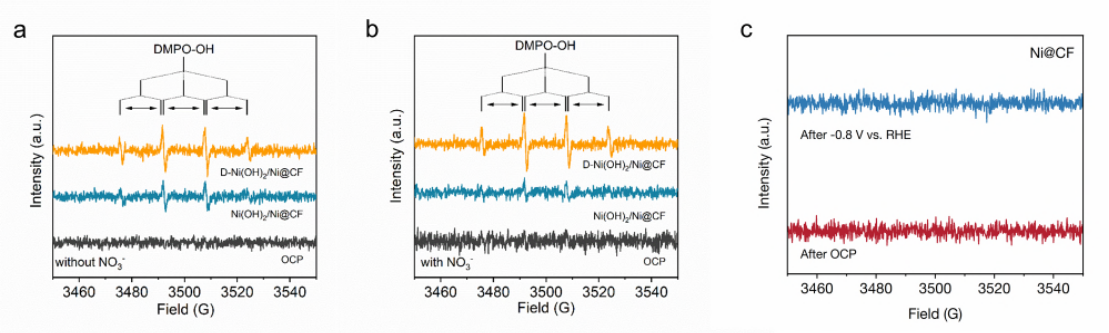

Figure 0-1. Quasi in-situ EPR spectra of collected electrolyte using D-$Ni(OH)_2$/Ni@CF and $Ni(OH)_2$/Ni@CF as electrocatalysts at -0.8 V vs. RHE in 1 M KOH without **(a)** and with **(b)** 0.1 M KNO_3, respectively (reported in the first manuscript). **(c)** Quasi in-situ EPR spectra of collected electrolyte using Ni@CF as electrocatalysts at -0.8 V vs. RHE in 1 M KOH (reported in the previous response).

Furthermore, we also evaluated Ni@CF catalyst under both NO_3RR and NO_2RR systems considering the three-step relay reaction mechanism on transition metal-based catalysts (Co, Fe, and Ni) [3] **(Figure 0-2a)**. In NO_3RR system, Ni@CF experienced a spontaneous oxidation to $Ni(OH)_2$, followed by subsequent reduction to Ni. The results indicated that the DMPO-OH signal only appeared during the NO_3RR process, implying the essential role of the surface reconstruction process of $Ni(OH)_2$ to Ni in facilitating the emergence of DMPO-OH, which is also consistent with the three-step relay mechanism on Ni proposed by the recent work [3]. Besides, considering that Fe and Co could spontaneously react with nitrate and undergo surface reconstruction under negative potential, we also performed measurements on $Fe(OH)_3$@CF and $Co(OH)_2$@CF, and the DMPO-OH species were also detected **(Figure 0-2b)**. However, such phenomenon does not exist on Pt, further confirming the interdependence of the surface reconstruction process with the DMPO-OH species. Additionally, to rule out the effects from Cu substrate, we synthesized the $Ni(OH)_2$@CC catalyst on carbon cloth. The

significant DMPO-OH signal confirmed that the effect is not due to the Cu foam substrate **(Figure 0-2c)**.

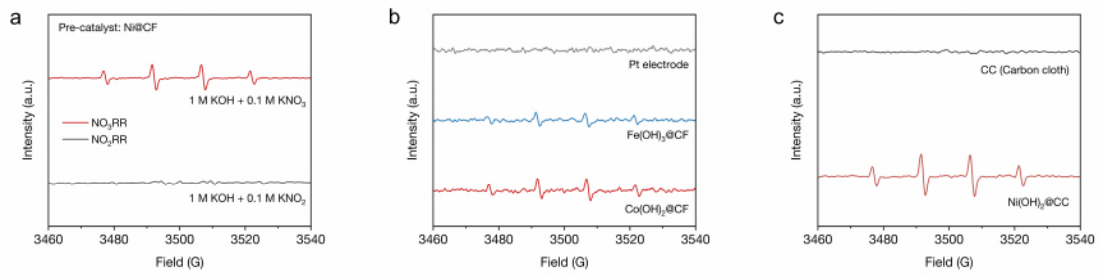

Figure 0-2. Quasi in-situ EPR spectra using Ni@CF as electrocatalysts in NO_3RR and NO_2RR systems. **(b)** Quasi in-situ EPR spectra on $Co(OH)_2$@CF, $Fe(OH)_3$@CF, and Pt electrode at -0.8 V vs. RHE. **(c)** Quasi in-situ EPR spectra on carbon cloth (CC) and $Ni(OH)_2$@CC at -0.8 V vs. RHE.

Thus, we concluded that the formation of DMPO-OH species may be originated from the nucleophilic addition of DMPO by active H_2O instead of the OH radicals **(Figure 0-3)**. This process following the Forrester-Hepburn mechanism (F-H mechanism) [1], and has been observed in diverse transition metal systems including Cu^{2+} [4], Fe^{3+} [5], and Ti^{4+} [6], etc. In our system, we have reported that the dynamic adsorption of OH on the Ni active site during the OH cycle could effectively activate interfacial H_2O dissociation. Thus, the interfacial H_2O activated during the OH cycle could be severed as the nucleophile and facilitated the formation of DMPO-OH specie, coupling with the electron transfer with $Ni^{2+} \rightarrow Ni^0$ on the electrode-electrolyte interface to complete the F-H process. Due to the thermodynamic stability of the transition metal hydroxide surface and the H_2O, this process could not occur spontaneously. Therefore, activation under a negative potential might be a crucial factor.

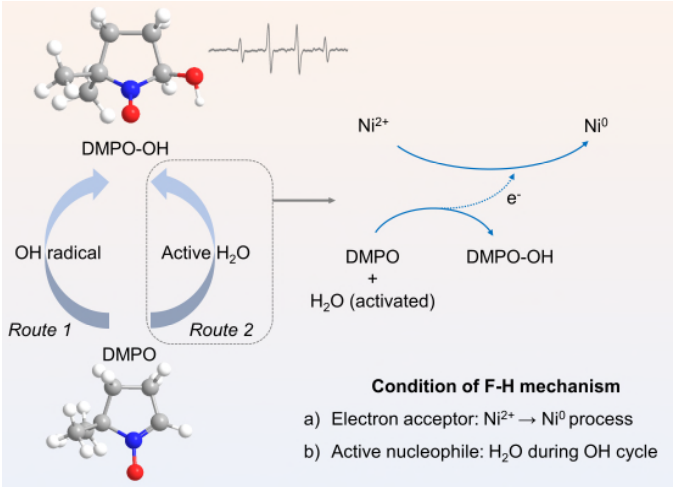

Figure 0-3. Schematic diagram of the understanding of DMPO-OH in this research.

Hence, the strength of the DMPO-OH signal might be also served as an indicator, which reflected the dynamics of surface reconstruction and activity of interface H_2O. In our study, D-Ni$(OH)_2$/Ni@CF exhibited a stronger signal than Ni$(OH)_2$/Ni@CF, indicating that D-Ni$(OH)_2$/Ni@CF possessed superior surface water activity and a faster conversion rate from Ni^{2+} to Ni^0. Finally, we revised the discussed in the manuscript as follows: *To quantitatively compare the concentration of surface active species, quasi in-situ EPR was performed. Four signal peaks with an intensity ratio of 1:2:2:1 were detected, which indicated the formation of DMPO-OH species. The DMPO-OH formed under negative potential might be attributed to the Forrester-Hepburn mechanism, where DMPO experienced nucleophilic addition by H_2O and coupled with an electron accepter ($Ni^{2+} \rightarrow Ni^0$). D-Ni$(OH)_2$/Ni@CF exhibited a stronger signal than Ni$(OH)_2$/Ni@CF, indicating the superior surface water activation and a faster conversion rate from Ni^{2+} to Ni^0 on D-Ni$(OH)_2$/Ni@CF. This was consistent with the conclusions reported by in-situ Raman results.*

Although our previous manuscript contained a misunderstanding of the DMPO-OH generation mechanism, the updated discussion did not affect the analysis of the catalytic mechanism presented in this work. On the contrary, it confirmed the results obtained from in situ Raman-FTIR analysis and other experiments. We greatly appreciate your suggestions, which have significantly improved the quality of the manuscript and deepened our understanding of surface chemical process.

[1] A.R. Forrester, et al. Spin Traps. A Cautionary Note. *J. Chem. Soc. C.* 701-703 (1971).

[2] L. Wang, et al. EPR Evidence for Mechanistic Diversity of Cu(II)/Peroxygen Oxidation Systems by Tracing the Origin of DMPO Spin Adducts. *Environ. Sci. Technol.* **56**, 8796-8806 (2022).

[3] S. Han, et al. Ultralow overpotential nitrate reduction to ammonia via a three-step relay mechanism. *Nat. Catal*. **6**, 402-414 (2023).

[4] W. Chamulitrat, et al. Evidence against the 1:2:2:1 quartet DMPO spectrum as the radical adduct of the lipid alkoxyl radical. *Arch. Biochem. Biophys.* **296**, 645-649 (1992).

[5] P. M Hanna, et al. When are metal ion-dependent hydroxyl and alkoxyl radical adducts of 5,5-dimethyl-1-pyrroline N-oxide artifacts? *Arch. Biochem. Biophys*. **296**, 640-644 (1992).

Inorganica Chimica Acta

[6] Y. Miura et al. Formation of the DMPO-OH adduct from Ti(IV) and DMPO in aqueous solution — the first ESR evidence. *Inorg. Chim. Acta*. **234**, 169-171 (1995).

1. In Fig. 1e-f, the author stressed that the strength of the Ni-O bond in $Ni(OH)_2$/Ni@CF is decayed than $Ni(OH)_2$@CF using the Wavelet transformation analysis. However, in the Fourier transformation analysis or the R space results shown in the inset of Fig. 1e, the intensity of the Ni-O bond about 1.8 Å in $Ni(OH)_2$/Ni@CF is stronger than that on $Ni(OH)_2$@CF. The Wavelet transformation and the Fourier transformation are only two different treatment methods on the same data. The conclusions should remain consistent. Besides, the color scale bars are missing in Fig. 1f and g.

We sincerely appreciate your questions about XAS in our paper. In the previous manuscript, there were some errors during the figure plotting of R-space intensity. Additionally, we observed that the surface Ni^0 signal on $Ni(OH)_2$/Ni@CF was very weak in the previous XAS results, despite showing clear signals in other characterization (TEM, XPS, and XRD). We assumed that most surface Ni^0 species oxidized before the XAS test due to improper preservation. To address this, the $Ni(OH)_2$/Ni@CF catalyst was carefully vacuum-sealed during the whole process, and all the XAS tests were re-performed immediately. We immediately applied for emergency access to Shanghai Synchrotron Radiation Facility (SSRF) and re-conducted a complete re-test for ensuring the accuracy of data. This allowed us to identify and correct the issues in sample preparation and test analysis. We sincerely appreciate your professional suggestions for the XAS section of this paper, and we have made revision to this section.

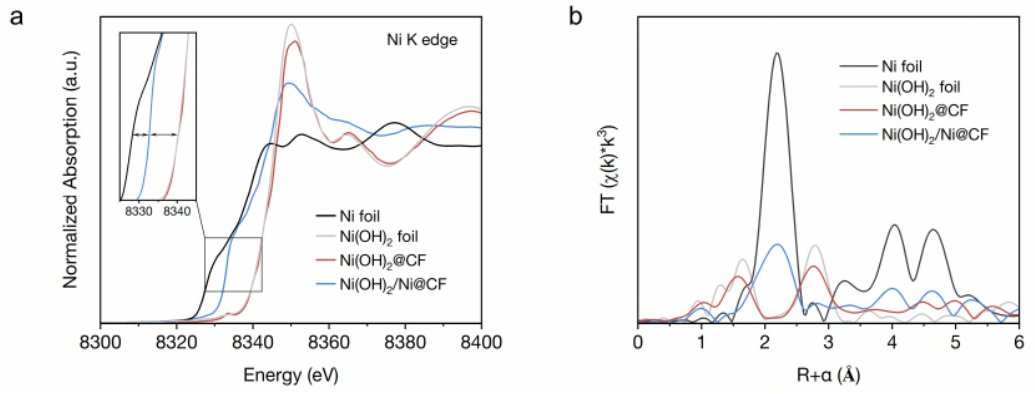

Figure 1-1. (a) Ni K-edge XANES spectra of $Ni(OH)_2$@CF and $Ni(OH)_2$/Ni@CF. **(b)** Corresponding Fourier transformed spectra.

In the X-ray absorption near-edge structure (XANES) spectra, it could be observed that $Ni(OH)_2$@CF exhibited relatively similar properties to that of $Ni(OH)_2$ foil, indicating that the surface of the catalyst maintains a stable $Ni(OH)_2$ structure **(Figure 1-1a)**. After electroreduction, the surface of $Ni(OH)_2$@CF reconstructed into $Ni(OH)_2$/Ni@CF. In the extended X-ray absorption fine structure (EXAFS) R-space spectra, $Ni(OH)_2$/Ni@CF exhibited the distinct Ni-Ni characteristic peak **(Figure 1-1b)**. Additionally, the fitting results also revealed related Ni-O and Ni-O-Ni peaks on $Ni(OH)_2$/Ni@CF. Although this signal was relatively weak, it was still evident in the absorption edge of XANES that the absorption edge of $Ni(OH)_2$/Ni@CF significantly located at a higher energy region compared to Ni foil, which confirmed that the $Ni(OH)_2$-Ni mixed phase of $Ni(OH)_2$/Ni@CF **(Figure 1-1a inset)**. Detailed fitting information for K-space and R-space was shown below **(Figure 1-2, Table 1-1).**

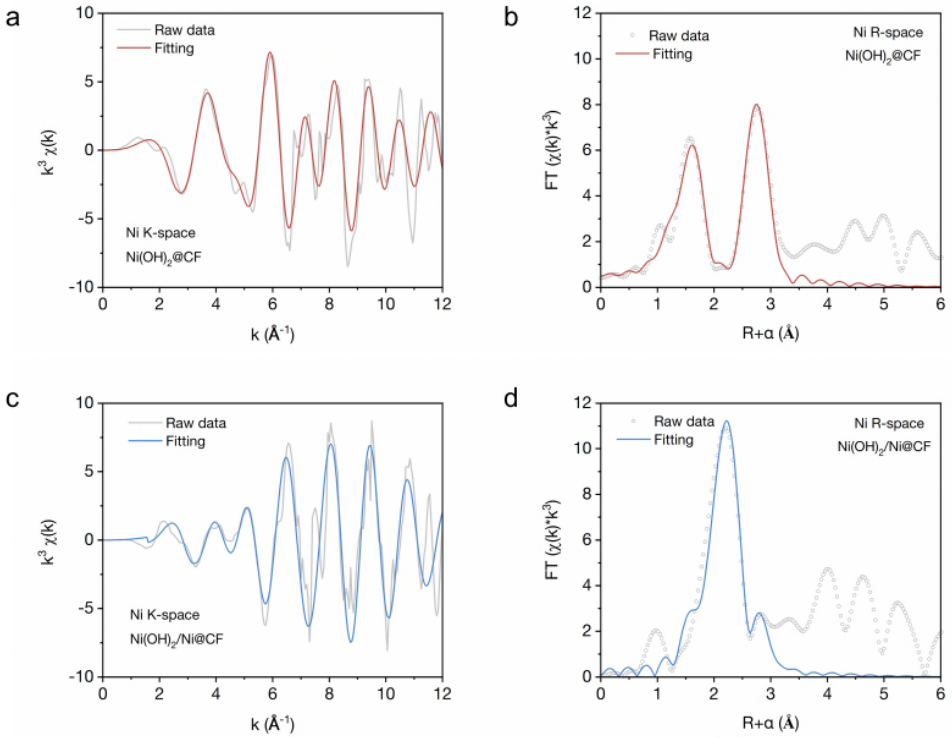

Figure 1-2. (a) The k^3-weighted extended EXAFS spectra and **(b)** the χ(R) space extended EXAFS spectra for the Ni K edge of $Ni(OH)_2$@CF. The red line represented the fitting spectra. **(c)** The k^3-weighted extended EXAFS spectra and **(d)** the χ(R) space extended EXAFS spectra for the Ni K edge of $Ni(OH)_2$/Ni@CF. The blue line represented the fitting spectra.

Table 1-1. Fitting parameters at the Ni K-edge of $Ni(OH)_2$@CF and $Ni(OH)_2$/Ni@CF.

Sample [a]	Path	N [b]	R [c] (Å)	σ^2 [d] ($\times 10^{-3}$ Å)	ΔE (eV)	R factor
$Ni(OH)_2$@CF	Ni-O	5.4±0.6	2.06±0.008	9.8±1.7	-3.4±0.9	0.017
	Ni-Ni (in $Ni(OH)_2$)	4.4±0.7	3.11±0.007	6.7±1.2		
$Ni(OH)_2$/Ni@CF	Ni-O	1.9±1.1	2.04±0.03	8.6±1.5	8.3±2.3	0.013
	Ni-Ni	3.5±1.2	2.43±0.01	6.2±2.5		
	Ni-Ni (in $Ni(OH)_2$)	1.6±2.8	3.09±0.04	7.2±1.3		

[a] S^0 was fixed as 1.0. [b] N is the coordination number. [c] is the distance between absorber and backscatter atoms. [d] σ^2 is the Debye-Waller factor. R-factor is residual factor.

Additionally, we have also added the color scale bar in the figures of wavelet transformation in the revised manuscript **(Figure 1-3)**. The $Ni(OH)_2$@CF pre-catalyst exhibited similar characteristic to $Ni(OH)_2$ foil, which corresponding to the single scattering paths of Ni-O and Ni-Ni, respectively **(Figure 1-3 a and c)**. After electrocatalytic reduction, $Ni(OH)_2$@CF turned into $Ni(OH)_2$/Ni@CF, and the $Ni(OH)_2$/Ni@CF surface exhibited properties similar to those of Ni foil, dominated by the Ni-Ni single scattering path, though Ni-O signals (1-2 Å) were still present **(Figure 1-3 b and d)**. These results indicated that the reconstruction of $Ni(OH)_2$@CF results in the $Ni(OH)_2$-Ni mixed phase on $Ni(OH)_2$/Ni@CF, which was consistent with previous characterization results.

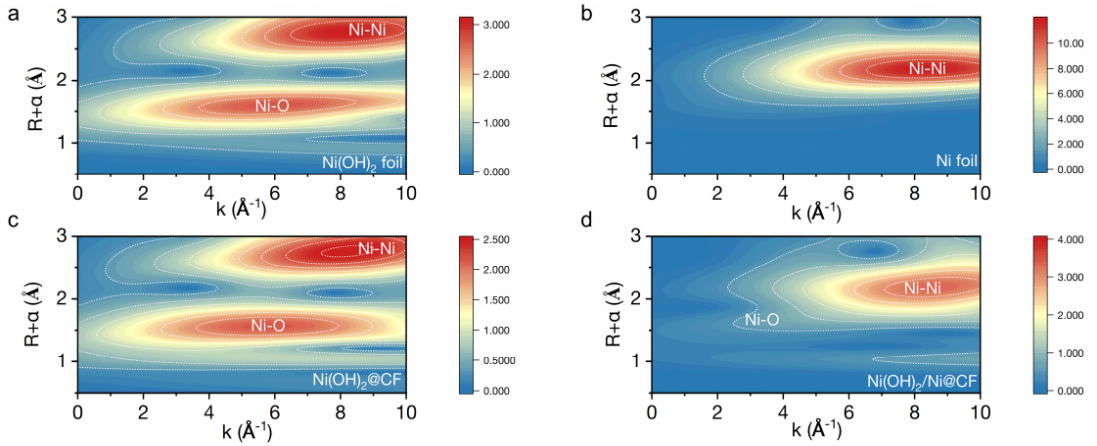

Figure 1-3. Wavelet transformation of **(a)** $Ni(OH)_2$ foil, **(b)** Ni foil, **(c)** $Ni(OH)_2$@CF, and **(d)** $Ni(OH)_2$/Ni@CF.

Thus, we have updated Fig. 1e-i and corresponding discussion in the manuscript: *To obtain the precise atomic-scale understanding of the catalyst, the local structure and valence state of $Ni(OH)_2$/Ni@CF and $Ni(OH)_2$@CF were comparatively examined through Ni K-edge X-ray absorption spectroscopy (XAS). $Ni(OH)_2$@CF exhibited similar peak characteristics to the $Ni(OH)_2$ foil in X-ray absorption near-edge structure (XANES) spectra, while $Ni(OH)_2$/Ni@CF displayed dominant metallic Ni-Ni bond in the extended X-ray absorption fine structure (EXAFS) R-space spectra. However, it was evident in XANES that the absorption edge of $Ni(OH)_2$/Ni@CF located at a higher energy region compared to Ni foil. Additionally, the wavelet transform (WT) of EXAFS revealed that $Ni(OH)_2$/Ni@CF exhibited both the metallic Ni-Ni bond signal and the Ni-O signal (1~2 Å). To precisely determine the Ni valence state, the average oxidation states was fitted by taking the valence of Ni (0.00) and $Ni(OH)_2$ (2.00) at 0.4 of normalized absorption as standards from Ni K-edge XANES. The nominal valence state of Ni in $Ni(OH)_2$/Ni@CF (+0.35) was located between $Ni(OH)_2$ (+2.00) and Ni (0.00). Overall, the XAS result confirmed that a significant amount of Ni^0 species was generated on the surface after electroreduction, while the mixed state of $Ni(OH)_2$/Ni was still retained.*

2. In Fig. 3h and I, the selected potential range is from +0.7 V to -0.1 V. What is the purpose of performing the EIS test from +0.7 V? Especially, the bode plots for D-$Ni(OH)_2$/Ni@CF is confusing. There is no obvious pattern. For example, is the phase angle for low low-frequency part is obvious than the high-frequency part for D-$Ni(OH)_2$/Ni@CF between +0.7 V to +0.5 V?

Thank you very much for the valuable feedback. Herein, we hoped to identify pivotal points in the surface behavior by using *Operando* EIS test. Given that the theoretical potential of NO_3RR stands at +0.69 V vs. RHE (pH=14) [1], the potential range from +0.7 to -0.1 V vs. RHE encompasses the transition from electrochemical double-layer capacitor (EDLC) behavior to electrochemical reduction on the catalyst surface. However, we recognized that this range may be overly broad, considering that D-$Ni(OH)_2$/Ni@CF and $Ni(OH)_2$/Ni@CF displayed EDLC behavior when the potential exceeded 0.5 V vs. RHE, and electrochemical reduction behavior below 0 V vs. RHE. Thus, we have adjusted the range to +0.5~0 V vs. RHE to enhance the clarity and conciseness of the data.

Moreover, we observed some fluctuation in the low-frequency region during the test over D-Ni(OH)$_2$/Ni@CF, which may be caused by the workstation. To address this, we reconduct the experiment using a new electrochemical workstation (CHI760e, same as the previous workstation) and re-performed the EIS measurements. The results showed a notable transitioning from the EDLC behavior to electroreduction behavior at +0.3 V vs. RHE over D-Ni(OH)$_2$/Ni@CF **(Figure 2-1a)**. Such transition was only observed upon potential reduce to +0.2 V vs. RHE on Ni(OH)$_2$/Ni@CF, demonstrating the lower onset potential and better catalytic performance of D-Ni(OH)$_2$/Ni@CF **(Figure 2-1b)**. Repeated experiments confirmed consistent results and the reproducibility of our experiments.

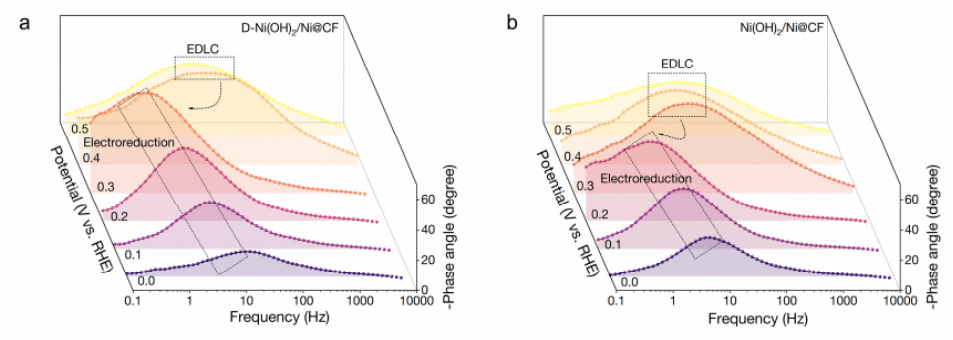

Figure 2-1. *Operando* EIS plots from 0.5 V vs. RHE to 0 V vs. RHE of (a) D-Ni(OH)$_2$/Ni@CF and (b) Ni(OH)$_2$/Ni@CF with a frequency range from 0.1 Hz to 10 kHz.

Thus, we have updated Figures and corresponding discussion in the manuscript: *To analyze the electrochemical dynamics of the catalyst surface, Operando EIS was performed during NO_3RR. The peaks in the high-frequency region corresponded to the charging process of the electrochemical double-layer capacitor (EDLC), while the peaks in the low-frequency region were associated with the electroreduction process. It was observed that a notable transition from the EDLC behavior to electroreduction behavior at +0.3 V vs. RHE over D-Ni(OH)$_2$/Ni@CF, much higher than that over Ni(OH)$_2$/Ni@CF (+0.2 V vs. RHE), which implied the lower onset potential and better catalytic performance of D-Ni(OH)$_2$/Ni@CF.*

[1] S. Han, et al. Ultralow overpotential nitrate reduction to ammonia via a three-step relay mechanism. *Nat. Catal*. **6**, 402-414 (2023)

3. In Figures 4b and d, the peaks at 2915 cm^{-1} and 2849 cm^{-1} were assigned to H-N-H. As the IR vibration at this range is usually related to vibration in C-H (J. Phys. Chem. 1996, 100,

25, 10664-10672), the authors should provide references or more experiments for support their conclusion.

Thanks for this question. For the identification of IR peaks at 2915 cm^{-1} and 2849 cm^{-1}, we referred and cited the previous articles about NO_3RR [1-2]. The peaks at ~2900 cm^{-1} were detected and were assigned to the *NH species in previous study. Furthermore, we meticulously scrutinized the *Method* part in these articles. We noted that all in-situ FTIR tests in these articles utilized either glassy carbon electrodes or carbon cloth electrodes, which likely accounted for the signal at ~2900 cm^{-1}. It is conceivable that during the experiment, partial detachment of the catalyst might have occurred, leading to the exposure of the glassy carbon or carbon cloth electrode to infrared light. Such exposure could have resulted in the formation of the C-H signal through the adsorption of intermediate H species. Thus, we repeated the in-situ FTIR experiment.

Firstly, we conducted in-situ FTIR tests by utilizing KOH electrolyte on a glassy carbon electrode. The signal peaks at 2915 and 2849 cm^{-1} could be observed even in environments lacking a nitrogen source **(Figure 3-1a)**. Thus, it was plausible to attribute the C-H vibration signal to the H_2O dissociation behavior on the glassy carbon electrode at -0.8 V vs RHE. This observation aligns with trends observed in electrolytes containing nitrogen sources **(Figure 3-1b)**. We express our gratitude for your inquiries and extensive chemical expertise, which have provided valuable insights into the intricate peaks observed in in-situ FTIR analysis.

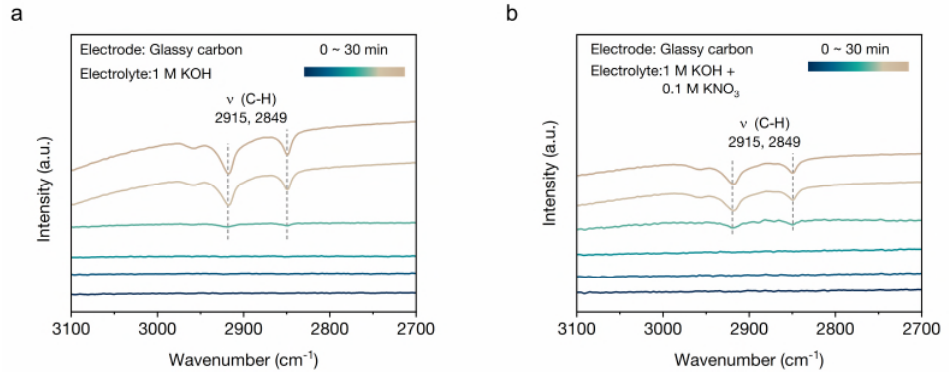

Figure 3-1. Time-dependent in-situ electrochemical FTIR spectra at -0.8 V vs. RHE over glassy carbon electrode with the electrolyte of **(a)** 1 M KOH and **(b)** 1 M KOH + 0.1 M KNO_3.

To address this issue, an updated ink was employed to enhance the adhesion of the catalyst to the glassy carbon electrode. Specifically, the ratio of Nafion and solvent was optimized, followed by drying with an infrared lamp. Subsequently, we conducted in-situ FTIR

analysis, and the result revealed that the electrode maintained stable for 45 minutes, with only very slight C-H signal at the 45 minutes **(Figure 3-2a)**. To further corroborate this, polarization curves were measured, demonstrating that the current density exhibited negligible decrease within the 45 minutes of electrolysis **(Figure 3-2b)**. Given that our FTIR analysis was conducted within 30 minutes, the combined results from in-situ FTIR and LSV tests affirmed the stability of our catalyst during in-situ FTIR analysis.

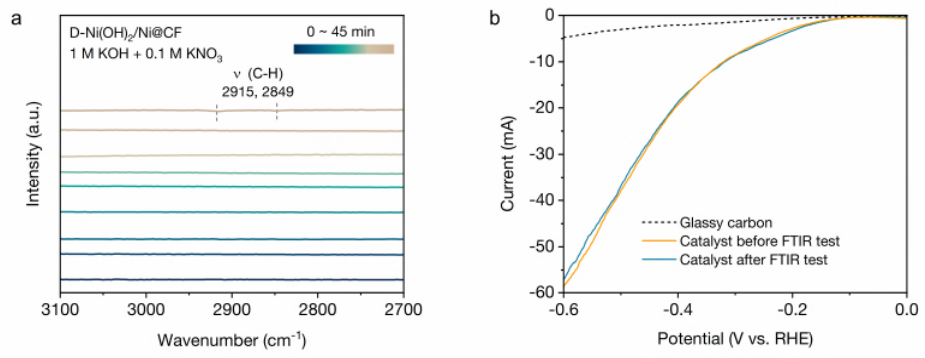

Figure 3-2. (a) Time-dependent in-situ electrochemical FTIR spectra (3100~2700 cm^{-1}) at -0.8 V vs. RHE over D-$Ni(OH)_2$/Ni@CF with the electrolyte of 1 M KOH + 0.1 M KNO_3. **(b)** Polarization curves of glassy carbon electrode, D-$Ni(OH)_2$/Ni@CF before FTIR test and D-$Ni(OH)_2$/Ni@CF after 45-min FTIR test.

Furthermore, we reconducted the in-situ FTIR test, and the results were consistent with our previous conclusions **(Figure 3-3)**. FTIR peaks located at ~1650 cm^{-1} were attributed to the OH species, while peaks located at 3005 and 3220 cm^{-1} were assigned to N-H species [3-5]. Notable peak signals corresponding to N species and interface OH species were observed at the onset of the reaction on D-$Ni(OH)_2$/Ni@CF and gradually strengthen with the reaction, implying the faster reconstruction and reaction kinetics over D-$Ni(OH)_2$/Ni@CF to promote water dynamics and proton transfer.

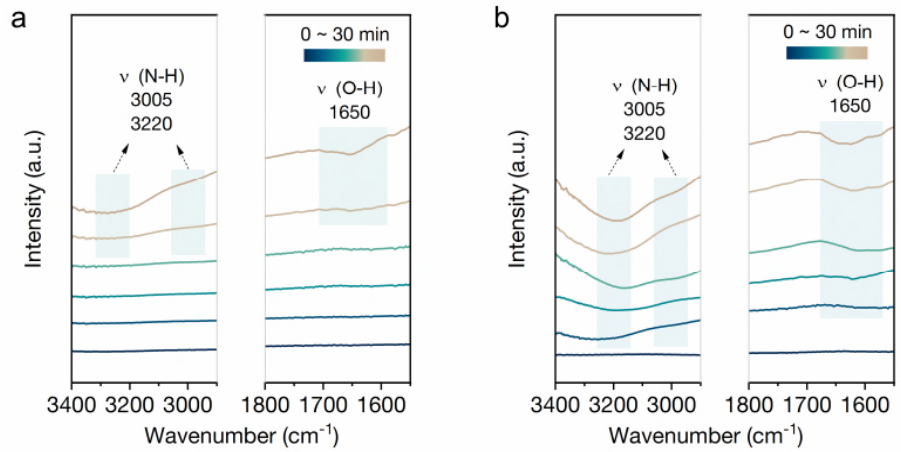

Figure 3-3. In-situ electrochemical FTIR spectra at -0.8 V vs. RHE of **(a)** $Ni(OH)_2$/Ni@CF and **(b)** D-$Ni(OH)_2$/Ni@CF with a time scale of 0~30 min.

Thus, we have updated Fig. 4b and Fig. 4d in the manuscript, and added references related to FTIR peak attribution (Ref 24, 37, 38 in the manuscript). Thank you very much for your professional advice, which has significantly improved the quality of the manuscript.

[1] Z. Gong, et al. Regulating surface oxygen species on copper (I) oxides via plasma treatment for effective reduction of nitrate to ammonia. *Appl. Catal. B-Environ*. **305**, 121021 (2022).

[2] L. Qin, et al. Electrochemical NO_3^- Reduction Catalyzed by Atomically Precise $Ag_{30}Pd_4$ Bimetallic Nanocluster: Synergistic Catalysis or Tandem Catalysis? *ACS Nano*. **17**, 12747-12758 (2023).

[3] S. Han, et al. Ultralow overpotential nitrate reduction to ammonia via a three-step relay mechanism. *Nat. Catal*. **6**, 402-414 (2023).

[4] B. Zhan, et al. Defect-induced triple synergistic modulation in copper for superior electrochemical ammonia production across broad nitrate concentrations. *Nat. Commun*. **15**, 2816 (2024).

[5] W. Liao, et al. Sustainable conversion of alkaline nitrate to ammonia at activities greater than 2 A cm^{-2}. *Nat. Commun*. **15**, 1264 (2024)

4. In Figure S35, the Raman data seems strange. The peak looks like a broken line. The sampling step should be adjusted.

Thank you very much for these valuable suggestions to help us promote the manuscript. In our previous in-situ Raman test, we utilized a relatively sparse sampling step, so the

expressed peak looked not well. To address this issue and enhance the quality of the manuscript, we have re-performed all the in-situ Raman test, employing a more refined sampling frequency. All updated information was depicted in **Figure 4-1**. Upon comparison with the previous in-situ Raman results, we have observed no discernible alterations in the new test.

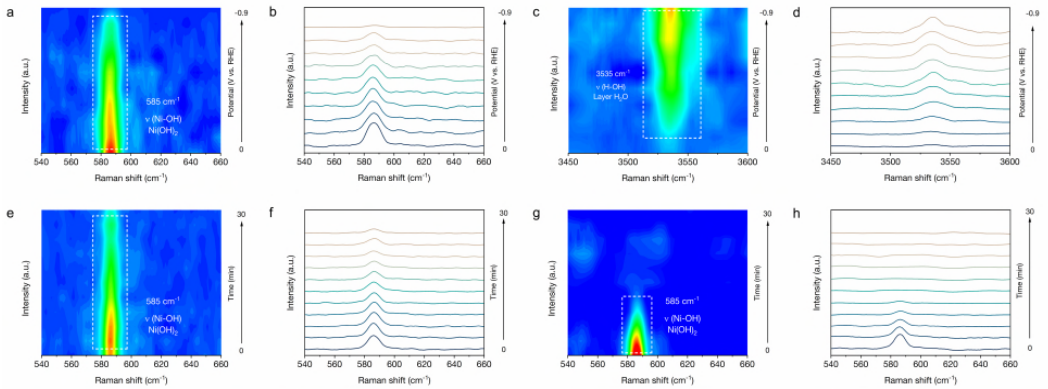

Figure 4-1. All figures and raw data related to in-situ Raman measurements in this article. **(a), (c)** Potential-dependent in-situ electrochemical Raman spectra of $Ni(OH)_2$/Ni@CF from 0 to -0.9 V vs. RHE in the electrolyte with 1 M KOH + 0.1 M KNO_3 and **(b), (d)** corresponding raw data. Time-dependent in-situ electrochemical Raman spectra at -0.8 V vs. RHE of **(e)** $Ni(OH)_2$/Ni@CF and **(g)** D-$Ni(OH)_2$/Ni@CF with a time scale of 0~30 min and **(f), (h)** corresponding raw data.

Thus, we have updated Fig. 2a, Fig. 4a, and Fig. 4c in the manuscript **(Figure 4-2)**. Your professional advice is very important in enhancing the quality of the manuscript, and we greatly appreciate your advice.

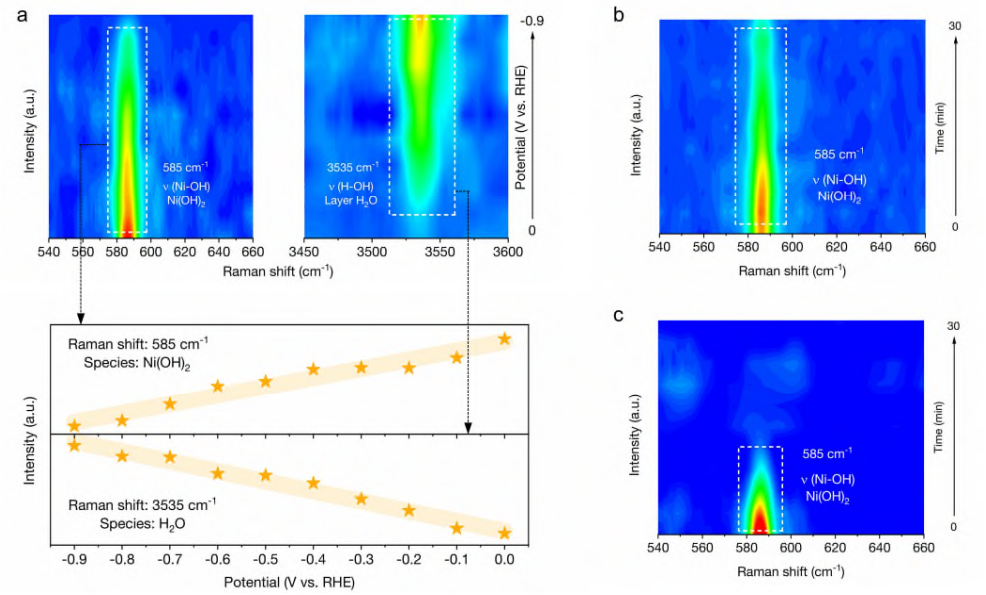

Figure 4-2. **(a)** Updated figure 2a in the manuscript. **(b)** Updated figure 4a in the manuscript. **(c)** Updated figure 4c in the manuscript.

5. The TEA of the generated NH_3 production process seems meaningless. Why the electrochemical system cost was calculated to be 968 $/kW? Based on what? It would be better if the authors provided a detailed calculation process. Considering the stability duration of D-Ni(OH)$_2$/Ni@CF is only 24 h, the calculation method seems suspectable.

Thank you for your suggestions on improving the quality of this article. Previously, the electrochemical system in the calculation model was relatively simple and estimated based on lab-customized devices in the TEA section. In the revised manuscript, we have supplemented more details about the cost of the whole system, particularly revising the electrochemical system cost based on extensive research and industrial reports. Furthermore, we have also considered catalyst replacement due to the deterioration.

We built a more elaborate TEA model of NO_3RR process inspired by previous studies in electrolyzers and electrocatalysis, where the NO_3RR system was reasonable scaled up to industrial levels [1-3]. The potential distributed NH_3 yield was assumed at a scale of 1 t d^{-1}. The cost of this process mainly consisted of capital cost and operational cost. To consider the effect of stability and activity of the catalyst on the cost of electrolyzer, we assumed that the catalyst could operate for 500 h with the average FE of 85%, and investigated its effect on the NH_3 production cost (e.g variation of FE from 70% to 100%). The lifetime of the whole nitrate electrolysis system was assumed of 20 years. The electrolyzer operation parameters were based on the performance of our prepared catalyst **(Table 5-1)**. Without considering ohmic losses etc, the cell voltage (V) in our experiment was set as 1.23-(-0.8) = 2.03 V. An operation of 7000 hours per year for the electrochemical system was assumed [1]. The electricity was assumed to be 0.03 $/kWh [1]. To achieve 1 t d^{-1} capacity, the needed total electrolyzer area (A_{ele}) which is normally contributed by multiple electrolyzer stacks was calculated as follows [1]:

$$A_{ele} = (\text{yield} \times n_{NH3} \times F) / (j \times \text{Average FE}) \quad (1)$$

Where yield represented the designed annual NH_3 production (1 t d^{-1}), n_{NH3} represented the number of electron transfers (8 for NO_3RR), F represented Faraday constant (96,485 C mol^{-1}). The cost of the electrolyzers was mainly composed of cathode material (e.g Ni & Cu), anode

metarial (Pt), ion exchange membranes, bipolar plates, end plates and tie rods. Each component's replacement time and cost parameters were listed **(Table 5-2)**. The current market metal price was also considered for catalysts used for cathode and anode materials [1]. For catalysts, the replacement cost (C_{re}) was calculated as follows [1]:

$$C_{re,i} = P_m \times LM \times A_{ele} \quad (2)$$

Where P_m represented the current market metal price, LM represented the loading mass per unit area. The cost of bipolar plates, end plates or tie rods ($/kW) was estimated [4], where reference electrolyzer operated at V_{ref} (1.9 V) and j_{ref} (2 A cm^{-2}). The cost was calculated as follows based on DOE [5]:

$$\text{Cost } (\$\ m^{-2}) = \text{Cost } (\$\ kW^{-1}) \times V_{ref} \times j_{ref} \quad (3)$$

Based on calculated results above, the capital cost of electrolyzers in its 20-year lifetime was calculated as follows:

$$C_{ele} = \sum_i C_{re,i} \times n_i \quad (4)$$

Where $C_{re,i}$ represented the replacement cost of i ($, i = catalysts, membrane, plates or tie rods), n_i represented the replacement time of i in 20 years. The electrolyzer cost per kW ($C_{ele\ per\ kW}$) considering material replacement was calculated as 1071 $ kW^{-1}.

The annual NH_3 yield ($yield_{NH3}$) was calculated to be 291.7 t yr^{-1} and the annual anode O_2 yield ($yield_{O2}$) was calculated to be 1,098 t yr^{-1} [1]. The electrolyzer electricity cost (C_{ee}) under 0.03 $ kWh^{-1} was calculated to be 263,562 $ yr^{-1}. Other costs (BoP, maintenance, etc) were estimated based on other literatures and listed in **Table 5-3**. The nitrate electrolysis system cost to produce 1 t NH_3 ($C_{ammonia}$) was calculated by total capital cost ($C_{cap,tot}$) and annual operational ($C_{op,tot}$) as follows:

$$C_{ammonia} = (C_{cap,tot} + C_{op,tot} \times 20) / (\text{ yield} \times 20) = 1{,}487\ \$\ t_{NH3}^{-1} \quad (5)$$

The total revenue (R_{tot}) was calculated as follows [2]:

$$R_{tot} = (P_{ammonia} \times yield_{NH3} + P_{oxygen} \times yield_{O2}) / yield_{NH3} = 1{,}156\ \$\ t_{NH3}^{-1} \quad (6)$$

Where $P_{ammonia}$ represented the market price of ammonia (290 $ t^{-1}) [6], P_{oxygen} represented the market price of oxygen (230 $ t^{-1}) [7]. Sensitivity analysis was performed by varying different parameters of ±50%, including electricity, cell performance and the designed NH_3 yield etc (Operation time and FE only vary of -50 %, cell voltage only vary of +50 %).

Table 5-1. Electrolyzer operation parameters

	Values	Units	Ref. & Notes
Designed ammonia yield, yield	1,000	kg d^{-1}	Assumed
Current density, j	~0.6	A cm^{-2}	Experimental
Average FE	85	%	Assumed
Cathode potential	-0.8	V	Experimental
Catalyst duration, t	500	h	Assumed
Electrolyzer area needed, A_{ele}	1,030,426	cm^2	Equation (1)
Operation time	7000	h yr^{-1}	Assumed

Table 5-2. Parameters and costs for the electrolyzer.

Component	Replacement time	Cost parameters
Ni	Based on operational time	20430 \$ t^{-1} [8] 63 g m^{-2} from experiment
Cu		3.815 \$ lbs^{-1} [8] 550 g m^{-2} from experiment
Pt	1 time per 2 yrs	974 \$/tr.oz [8] 7 g m^{-2} [3]
Membrane	1 time per 2 yrs [9]	750 \$ m^{-2} [9]
Bipolar plate	1 time per 7 yrs [4]	535 \$ m^{-2} [4, 5]
End plate		16 \$ m^{-2} [4, 5]
Tie rods		16 \$ m^{-2} [4, 5]

Operational time: (7000 h) / (500 h) y^{r-1}. Separating the cathode does not damage the membrane due to the CF substrate)

Table 5-3. Cost components for the nitrate electrolysis system.

	Values	Units	Ref. & Notes
	Capital cost		
C_{ele}	1,344,768		This study
$C_{cap,\ BOP}$	860,652	$	64 % of C_{ele}[1]
$C_{cap,\ tot}$	2,205,420		
	Operational cost		
C_{chem}	0		Waste water [2]
C_{ee}	263,562		Electrolyzer electricity
$C_{op,\ PS}$	26,356	$ yr^{-1}	10 % of C_{ee} [2]
C_m	33,619		2.5 % of C_{ele} [1]
$C_{op,\ tot}$	323,537		

To ensure the stability of D-Ni(OH)$_2$/Ni@CF during repeated experiments, we reconducted the experiments and extended the cycle to 50, and assessed its declination of the activity, which helps to provide certain reference for mentioned-above analysis **(Figure 5-2a)**. The electrolytic cell was placed in 25 ℃ water bath to prevent the fluctuations in catalyst performance due to environment temperature variations. A slight decline in the average FE was observed from the initial 24 hours to entire 50-hour interval **(Figure 5-2b)**. The average FE of 1-50 cycles was 97.26%, dropping about 1.5% compared to 1-24 cycles (98.72%), which showed a potential for 500-hour operation.

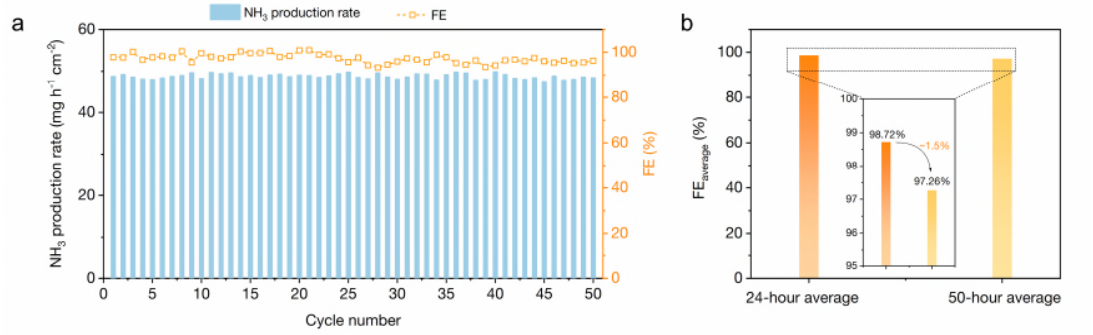

Figure 5-2. (a) Repeat stability test over D-Ni(OH)$_2$/Ni@CF for 50 cycles (1 hour per cycle). **(b)** Average FE of 1-24 h and 1-50 h

The above are full details of the supplementary TEA calculations. Although this work mainly focuses on the mechanism on the NO_3RR interface, we are interested in the future potential application. Thus, we have updated the corresponding discussion in the manuscript: *Techno-*

economic analysis (TEA) combined with sensitivity analysis was carried out to ascertain the economic potential. Under the current catalyst performance, the NH_3 production cost by NO_3RR was calculated to be 1,487 \$ t^{-1}. Given its sensitivity to the electricity, the route of NH_3 synthesis through NO_3RR remains appealing with further improvements on renewable energy, thereby exhibiting promising application potential. We believed that including your valuable question could provide a valuable reference for the calculation of electrocatalytic TEA.

[1] H. Shin, et al. *Nature Sustain.* **4**, 911-919 (2021).

[2] K. Fan, et al. *Nat Common.* **13**, 7958 (2022).

[3] A. Mayyas, et al. National Renewable Energy Laboratory (NREL), https://www.nrel.gov/docs/fy19osti/72740.pdf.

[4] A. Badgett, et al. National Renewable Energy Laboratory (NREL), 2024, https://www.nrel.gov/docs/fy24osti/87625.pdf.

[5] D. Peterson, et al. DOE hydrogen and fuel cells program record 19009: Hydrogen production cost from PEM electrolysis-2019, US Department of Energy, 2020, https://www.hydrogen.energy.gov/pdfs/19009_h2_production_cost_pem_electrolysis_2019.pdf.

[6] ChemAnalyst, Ammonia price trend and forecast, https://www.chemanalyst.com/Pricing-data/ammonia-37.

[7] ChemAnalyst, Oxygen price trend and forecast, https://www.chemanalyst.com/Pricing-data/oxygen-1575.

[8] Trading Economics, https://tradingeconomics.com.

[9] A. Iizuka, et al. *Sep. Purif. Technol.* **101**, 49-59 (2012).

Thank you very much for these valuable suggestions to help us get insight into the mechanism. We have completely updated the manuscript. Sincerely thank you for improving the quality of this manuscript!

REVIEWERS' COMMENTS

Reviewer #1 (Remarks to the Author):

This manuscript can be accepted without further revisions.